

# Journal of Materials Chemistry B

Accepted Manuscript



This is an *Accepted Manuscript*, which has been through the Royal Society of Chemistry peer review process and has been accepted for publication.

*Accepted Manuscripts* are published online shortly after acceptance, before technical editing, formatting and proof reading. Using this free service, authors can make their results available to the community, in citable form, before we publish the edited article. We will replace this *Accepted Manuscript* with the edited and formatted *Advance Article* as soon as it is available.

You can find more information about *Accepted Manuscripts* in the [Information for Authors](#).

Please note that technical editing may introduce minor changes to the text and/or graphics, which may alter content. The journal's standard [Terms & Conditions](#) and the [Ethical guidelines](#) still apply. In no event shall the Royal Society of Chemistry be held responsible for any errors or omissions in this *Accepted Manuscript* or any consequences arising from the use of any information it contains.

## ARTICLE

# Peptide-Based Biomaterials. Linking L-Tyrosine and Poly L-Tyrosine to Graphene Oxide Nanoribbons

Cite this: DOI: 10.1039/x0xx00000x

J. M. González-Domínguez,<sup>a</sup> F. A. Gutiérrez,<sup>b</sup> J. Hernández-Ferrer,<sup>a</sup> A. Ansón-Casaos,<sup>a</sup> M. D. Rubianes,<sup>b</sup> G. Rivas<sup>b\*</sup> and M. T. Martínez<sup>a\*</sup>

Received 00th January 2012,

Accepted 00th January 2012

DOI: 10.1039/x0xx00000x

[www.rsc.org/](http://www.rsc.org/)

Peptide-based biomaterials are being studied actively in a variety of applications in materials science and biointerface engineering. Likewise, there has been ongoing exploration over the last few decades, into the potential biological applications of carbon nanomaterials, motivated by their size, shape, structure and their unique physical and chemical properties. In recent years, the functionalization of carbon nanotubes and graphene has led to the preparation of bioactive carbon nanomaterials that are being used in biomedicine as structural elements and in gene therapy and biosensing. The present study, proposes different strategies for the bonding of L-Tyrosine and the homopolymer Poly-L-Tyrosine, to graphene oxide nanoribbons (GONRs). The covalent attachment of L-Tyrosine was undertaken by amidation of the  $\alpha$ -amine group of tyrosine with the existing carboxylic groups in GONR and by means of esterification through phenol nucleophiles contained in their side-chains. In both cases use was made of protective groups to address the functionalization to the desired reactive groups. The linking of GONRs to the PTyr was attempted according to two different strategies: either by ester bonding of commercial PTyr through their phenol side groups or, by *in situ* ring-opening polymerization of an N-carboxyanhydride tyrosine derivative (NCA-Tyr) with Tyr-functionalized GONRs. These biofunctionalized nanomaterials were characterized by Raman and infrared spectroscopy, X-ray photoelectron spectroscopy, thermogravimetric analysis, transmission electron microscopy, fluorescence and electrochemical techniques. On the basis of their properties, prospects for the potential utilization of the prepared hybrid nanomaterials in different applications are also given.

## Introduction

The rapidly evolving field of nanotechnology presents constant demands on the scientific community to advance and create new materials. The ability to synthesize and manipulate matter at the nanoscale can have significant impact in a number of fields, including medicine (diagnostics, drug delivery, tissue engineering), electronics (memory storage, nanoelectronics, quantum computers, novel semiconductor, and optoelectronic devices), bioseparation and catalysis.

Graphene, a novel two-dimensional nano-material composed of  $sp^2$ -bonded carbon atoms, possesses a number of extraordinary electronic, optical, thermal and mechanical properties.<sup>1-5</sup> Graphene oxide, reduced graphene oxide, graphene nanoribbons, few-layered graphene and graphene quantum dots are prominent members of this family and are extensively used in nanotechnology as building blocks for diverse applications. With the rapid development of synthesis and functionalization approaches, graphene and its related derivatives have shown outstanding potential in many fields—such as nanoelectronics,<sup>6</sup>

composite materials,<sup>7-8</sup> energy technology (for example, fuel cells, supercapacitors),<sup>9-10</sup> sensors,<sup>11-12</sup> and catalysis,<sup>13</sup> as it has been summarized in a number of review articles.<sup>14-20</sup> In recent years, graphene derivatives have been extensively explored for widespread biological applications including biosensing platforms, DNA/RNA carriers, and photothermal therapy as a consequence of its pharmacokinetic properties, the ability to effectively cross biological barriers, near infrared absorption and capacity for facile biological/chemical functionalization.<sup>21</sup> Moreover, proteins and peptides have received a great deal of attention as components of higher-order materials for medicinal applications<sup>22</sup> and lot of exciting work is also being performed in the field of small molecular-weight, peptide-engineered materials. The use of peptides, proteins and such protein assemblies as nanotubes, scaffolds, and nanowires has shown much promise as a bottom-up approach to the development of novel bionanosystems.<sup>21</sup> Peptides are also of interest because of the broad chemical diversity (acidity and hydrophobicity, among others) that can be achieved within a relatively compact

## ARTICLE

size. Furthermore, peptides impart a degree of robustness relative to proteins and antibodies, making possible their use in more extreme environments and long-term storage. Biomaterials design and engineering make use of hybrid approaches that combine the best qualities of synthetic materials with biologically active peptides.<sup>23–25</sup> New carbon nanostructured materials are particularly promising building blocks for biomaterial engineering and represents a new bottom-up approach for the development of novel nanosystems. To name a few examples, Li et al. have found stimuli-responsive properties using block co-polypeptide decorated single walled carbon nanotubes (SWCNTs),<sup>26</sup> while Battigelli et al.<sup>27</sup> have prepared peptide-based carbon nanotubes (CNTs) for mitochondrial targeting. Likewise, owing to their amphiphilic nature (consisting of “chained” aminoacids) polypeptides have been used as dispersing agents.<sup>28</sup> for CNTs The coupling of peptides and graphene offers a promising concept for components of sensors or nanocircuits as well as tissue scaffolds for regenerative medicine. One approach to mitigate the challenges of carbon nanostructures solubility and cytotoxicity is to modify these nanostructures with biomolecules. Since the functionalized graphene appears to be non-toxic for the cells<sup>29</sup>, it can be considered as a new tool for the delivery of peptides or proteins into cells. Tyrosine is being extensively used in the preparation of biomaterials. By way of example, L-Tyrosine-derived pseudo-polyamides<sup>30</sup> and L-tyrosine-based diphenolic monomers, polyiminocarbonates, polycarbonates and polyarylates<sup>31</sup> have shown considerable promise for application in implantable biodegradable orthopaedic devices and in bone-tissue engineering. Likewise, L-tyrosine-based polyurethane blends hold the potential for use in different biomaterial applications to fabricate a suitable material for different biomedical applications, particularly for the fabrication of tissue engineering scaffolds.<sup>32,33</sup> Huang et al. have explored the unique features of tyrosine in order to trigger supramolecular hydrogel formation and have prepared supramolecular hydrogels with reverse thermal gelation properties from (oligo)tyrosine-containing block copolymers.<sup>34</sup> It has also been reported<sup>35</sup> that tyrosine, as a component of block copolymers in ceramic composite xerogels, provides a remarkably broad and uniquely tunable range of mechanical and drug delivery properties under in vitro physiological conditions. Additionally, tyrosine-derived nanospheres have been used to enhance the topical skin penetration<sup>36</sup> of highly lipophilic model compounds and nanospheres formulated from L-tyrosine polyphosphate as a potential intracellular delivery device.<sup>37</sup>

This article is focused on the use of different strategies for the preparation of building blocks made from GONRs, with tyrosine (Tyr) and polytyrosine (PTyr) through covalent attachment or *in situ* polymerization of Tyr at the surface of GONRs. Hybrid materials leaving amine or phenolic terminal groups and materials with different PTyr content depending on the type of attachment have been obtained providing different alternatives for further potential applications of the resulting functional nanomaterials in biological settings.

## Experimental

### Materials and Reagents.

GONRs were synthesized by longitudinal oxidative unzipping of CNTs, using Tour's method.<sup>38,39</sup> Briefly, 150 mg of arc-discharge multiwall carbon nanotubes (MWCNTs)<sup>40</sup> were dispersed by bath sonication in 150 mL of concentrated H<sub>2</sub>SO<sub>4</sub>. Subsequently, the dispersion was heated up to 65°C for 120 minutes and after adding 750 mg of KMnO<sub>4</sub> the heating continued for 120 min. Then, the dispersion was poured onto 400 g of ice and 10 mL of H<sub>2</sub>O<sub>2</sub> solution was added. The reaction product was vacuum-filtered through a 3.0 μm polycarbonate membrane, dispersed in 150 mL of ultrapure water, flocculated with HCl, filtered through a 3.0 μm polycarbonate membrane, redispersed in 150 mL of ethanol, flocculated with 150 mL ether + 15 mL hexane and filtered through a 10.0 0-μm PTFE membrane. Finally, it was finally dried at 60°C in a vacuum oven for 24 h. O-Methyl-L-Tyrosine (Tyr-O-CH<sub>3</sub>), N-tert-Butoxycarbonyl-L-Tyrosine (N $\alpha$ -Boc-Tyr), PolyL-Tyrosine (PTyr, mol. Wt. 10000-40000), triphosgene, O-(Benzotriazol-1-yl)-N,N,N',N'-tetramethyluronium hexafluorophosphate (HBTU), ethyldiisopropylamine (EDIPA), trimethylsilyl iodide, (CH<sub>3</sub>Si), thionyl chloride and sodium dodecylbenzenesulfonate (SDBS), as well as organic solvents (in reagent grade) were obtained from Sigma-Aldrich or Acros and used without further treatments.

### Covalent Functionalization

The Tyrosine monomer was bound to the existing carboxylic groups of GONRs by means of two different strategies: either by amidation with  $\alpha$ -amino groups or by esterification with the phenolic groups present in L-Tyr, (Scheme 1). In order to drive the covalent linkage with the desired functionalities, and to minimize the feasible self-peptidic condensation amongst tyrosine molecules in the reaction conditions, use was made of convenient protective groups for the groups not involved in the reaction. For the amidation reaction the phenolic groups of Tyr

were protected as methoxy derivatives using Tyr-O-CH<sub>3</sub> and for the esterification reaction the  $\alpha$ -amino groups were protected with tert-butyloxycarbonyl (Boc) protective groups using the N $\alpha$ -Boc-Tyr reactant. PTyr was anchored to the GONRs using two different pathways: covalent functionalization by esterification using commercial PTyr (sample GONR-PTyr-Cov) and ring-opening polymerization of N-carboxyanhydride (NCA) derivatives of group-protected Tyr (NCA-Tyr-OCH<sub>3</sub>) in the presence of GONR-Tyr-NH<sub>2</sub> (sample GONR-PTyr-*in situ*), as displayed in Scheme 2. However, given the reactive nature of the oxygen species contained in GONRs we did consider the possibility of that other pathways might take place, such as epoxide-ring opening by terminal nucleophiles of Tyr derivatives<sup>42</sup> or acylation of hydroxyl groups. This has been taken into account in Schemes 1 and 2.

**AMIDATION REACTION (SAMPLE GONR-TYR-OH).** In a typical experiment, 100 mg of GONRs were placed in a round-bottom flask and bath-sonicated for 1h in an SDBS aqueous solution (0.5 wt% SDBS in deionized water). The resulting fine suspension was then transferred to a Schlenk flask and purged with Ar for few minutes, while stirring with a magnetic stirrer. The Ar atmosphere, set to a gentle continuous flow, and the magnetic stirring, were maintained inside the Schlenk flask throughout the whole functionalization process. The GONR dispersion was externally cooled with a water/ice bath until it reached 0°C. Afterwards, 300mg of HBTU and 2mL of EDIPA were added, and the reaction was allowed to continue at 0°C for 45min. Finally, 200mg (0.81 mmol) of Tyr-OCH<sub>3</sub> was incorporated and the reaction proceeded for 48h at room temperature. The reaction medium was thoroughly dialyzed against deionized water in a 5L tank while placed into 12kDa cutoff-sacks. After replacing the water many times, the sample was considered to be clean when no traces of SDBS or amidation reagents could be detected in the washing waters. Dialysis control was carried out by UV-Vis spectroscopy. As all species containing aromatic rings (e.g. Tyr derivatives, SDBS, HBTU) give off measurable signals in UV-Vis we monitored spectra of successive aliquots until no signals were appreciated. Finally, GONR-Tyr-OCH<sub>3</sub> was isolated by freeze-drying the as-obtained liquid medium. The deprotection of the phenol groups in the functionalization with Tyr-O-CH<sub>3</sub> was performed with CH<sub>3</sub>ISi, under the best conditions for methyl-protected phenols, as reported by Jung and Lyster.<sup>42</sup> Briefly, in a typical cleavage reaction, 100mg of GONRs functionalized with Tyr-O-CH<sub>3</sub> were mixed with 25mL of chloroform and slightly sonicated in ultrasonic bath. Then, 33mg of CH<sub>3</sub>ISi was incorporated and the mixture was refluxed at 50°C for 24h. Afterwards, the mixture was diluted in a 4-fold excess of methanol, vacuum-filtered through a 0.1 $\mu$ m pore size membrane, rinsed with diluted aqueous sodium bicarbonate, and finally dried.

**ESTERIFICATION REACTION (SAMPLE GONR-TYR-NH<sub>2</sub> AND GO-PTYR-COV).** 120mg of GONRs were placed in a round-bottom flask and dispersed in 10mL of anhydrous N,N'-

dimethylformamide (DMF), with the aid of an ultrasonic bath for 30min. After the addition of 24mL of thionyl chloride the mixture was refluxed at 120°C for 24h with constant magnetic stirring. These GONRs were vacuum-filtrated through a 0.1 $\mu$ m pore size Teflon membrane, thoroughly washed with anhydrous tetrahydrofuran (THF) and dried in vacuum at room temperature to obtain acyl chloride GONRs. Then, 100mg of freshly acyl-chlorinated GONRs were redispersed in 25mL of anhydrous DMF in an ultrasonic bath and the flask was purged with a continuous flow of Ar. 2mL of EDIPA was then added, followed by 0.81mmol of Tyr-OCH<sub>3</sub> or PTyr (in the latter case, the approximated molecular weight was 25000 g/mol). The reaction medium was allowed to react at 60°C for four days under Ar atmosphere. It was subsequently vacuum-filtrated through a 0.1 $\mu$ m pore size Teflon membrane and thoroughly washed with DMF and methanol. Finally, the functionalized GONRs were dried in vacuum at room temperature overnight. In order to cleave the Boc groups blocking the primary amines towards the GONR-Tyr-NH<sub>2</sub> sample, the powder obtained after esterification was redispersed in 1,4-dioxane with the aid of an ultrasonic bath. Concentrated HCl was then carefully added to achieve a final concentration of 4% v/v (HCl/dioxane), and the mixture was left at room temperature with constant magnetic stirring for 2h. The mixture was finally filtered in a 0.1 $\mu$ m pore size Teflon membrane, rinsed with 1,4-dioxane and diethyl ether, and dried under a vacuum at room temperature.

#### Ring-Opening Polymerization

**SYNTHESIS OF NCA-TYR-O-CH<sub>3</sub>.** NCA derivatization was carried out through a widely reported procedure using triphosgene.<sup>43,44</sup> It is important to note that triphosgene is a hazardous chemical that needs to be worked in the most strict anhydrous conditions. In a typical experiment, 0.65g of L-Tyr-O-CH<sub>3</sub>, and 0.46mg of triphosgene were placed in a Schlenk flask with 50mL of anhydrous 1,4-dioxane to avoid the phosgene formation and purged with Ar for few minutes, while stirring with a magnetic bar. An Ar atmosphere was set to a gentle continuous flow, and the stirring was maintained inside the Schlenk flask through the process. The mixture was then heated at 60 °C. The solution became progressively clear and all solids were fully dissolved after 3h. The NCA-Tyr-O-CH<sub>3</sub> was crystallized by pouring the reaction mixture into 500mL of hexane, and left overnight in a freezer. The as-obtained crystals were washed with n-hexane, dried under vacuum and stored in a refrigerator until use. C<sub>11</sub>H<sub>11</sub>NO<sub>4</sub> (calculated mass 221). <sup>1</sup>H-NMR (400 MHz, DMSO-d<sub>6</sub>):  $\delta$  9.04 (bs, 1H); 7.15 (d, J = 7.0 Hz, 2H); 6.87 (d, J = 7.0 Hz, 2H); 4.72 (dt, J = 4.7 Hz, 1H); 3.71 (s, 3H); 2.95 (t, J = 2.9 Hz, 2H). <sup>13</sup>C-NMR (100 MHz, DMSO-d<sub>6</sub>):  $\delta$  171.3, 158.8, 152.1, 131.2, 126.8, 114.2, 58.8, 55.4, 35.8 ppm. m/z (ESI MS<sup>+</sup>): experimental mass [M-1]<sup>+</sup> = 219.7 (See Figure S1 in supporting information for FTIR spectrum).

#### PEPTIDE HOMOPOLYMERIZATION (GONR-PTYR-*IN SITU*).

Peptide homopolymerization was performed under mild conditions, with a suitable initiator.<sup>44,45</sup> 120mg of GONR-Tyr-

$\text{NH}_4^+$  was placed in a round-bottom flask and dispersed in 25 mL of anhydrous DMF and 1 mL of EDIPA, with the aid of an ultrasonic bath for 30 min. Afterwards, 600 mg of NCA-Tyr-O- $\text{CH}_3$  was mixed with 10 mL of DMF and 1 mL of EDIPA. Both liquid fractions were transferred to a Schlenk flask and purged with Ar for a few minutes while stirring magnetically. Then 4 drops of octylamine or propylamine were added, and the system was heated up to 30 °C. Aliphatic primary amines are commonly employed as initiators in polymer synthesis, particularly when the polymerization mechanism undergoes ring-opening polymerization of NCA derivatives<sup>44</sup>. The Ar atmosphere set to a gentle continuous flow and magnetic stirring were maintained during the process. The reaction was allowed to continue for 48 h. The reaction product was vacuum-filtrated through a 0.1  $\mu\text{m}$  pore size Teflon membrane, washed with anhydrous THF and dried in oven at 30–40 °C. The deprotection of phenols from methyl protective groups was accomplished in identical manner as described for the GONR-Tyr-OH sample.

### Structural Characterization

Infrared spectroscopy (FTIR) measurements were carried out in a Bruker Vertex 70 spectrometer. The samples were prepared by mixing small amounts of the powder samples with spectroscopic-grade KBr and pressing to form pellets. X-ray photoelectron spectroscopy (XPS), was performed in an ESCAPlus Omicron spectrometer provided with a Mg anode (1253.6 eV) working at 150 W (15 mA, 10 kV), CASA software was used for the peak deconvolution. Shirley type baseline correction was applied. Thermogravimetric analysis (TGA) was carried out in a Setaram balance, model Setsys Evolution 16/18, under a nitrogen inert flow and a heating ramp of 10 °C  $\text{min}^{-1}$  in the range from room temperature to 800 °C. A model Q600 from TA Instruments coupled to a gas analysis system by mass spectrometer model THERMOSTAR QMS200 M3 was also used for TGA/MS. Micro-Raman spectroscopy was performed in a HORIBA Jobin Yvon spectrometer (model HR 800 UV) working with a green laser at 532 nm. For each material, 4–5 representative spectra of different sample zones were considered. Average particle size was determined in a Zeta Sizer Nano equipment (Malvern Instruments). Transmission electron microscopy was performed in a JEOL-200FXII equipment using C/Cu 200 mesh Lacey microscopy grids. Fluorescence spectroscopy was carried out in a Floromax-P Horiba Jobin Yvon equipment. The elemental analysis of the samples (as regards C, H, N and S wt%) was performed in a Carlo Erba Thermo Flash 1112 device using oven-dried and thoroughly milled samples. For a typical C, H, N and S determination, samples are burnt in pure oxygen at 950 °C in the presence of  $\text{V}_2\text{O}_5$ . Combustion products pass through an oxidant bed of CuO at 950 °C to be converted into  $\text{NO}_x$ ,  $\text{CO}_2$ , and  $\text{H}_2\text{O}$ . Then, a reducing bed of metallic Cu at 500 °C transforms  $\text{NO}_x$  into  $\text{N}_2$ . The gases were separated in a polar chromatographic column, and quantified by thermal conductivity.

### Electrochemical Characterization

The electrochemical experiments were performed with a TEQ04 potentiostat. The electrodes were inserted into the cell (BAS, Model MF-1084) through holes in its Teflon cover. Glassy carbon electrodes (GCE) either bare or modified with a given dispersion were used as working electrodes, while platinum and Ag/AgCl, 3M NaCl (BAS, Model RE-5B) were used as counter and reference electrodes, respectively. All potentials were referred to the latter.

**WORKING ELECTRODES PREPARATION.** The dispersions were prepared in the following way: 0.5 mg of GONR-Tyr- $\text{NH}_2$ , GONR-Tyr-OH, GONR-PTyr-Cov, or GONR-PTyr-*in situ* were mixed with 1.00 mL of  $\text{H}_2\text{O}/\text{EtOH}$  (50:50 v/v) and sonicated with an ultrasonic probe VCX 130W (Sonics and Materials, Inc.) of 20 kHz frequency with a titanium alloy microtip (3 mm diameter) for 3 minutes using 50% amplitude. GCE electrodes were polished with alumina slurries of 1.0, 0.30, and 0.05  $\mu\text{m}$  respectively for 2 min each. Before deposition of the dispersion, the electrode was cycled in a 0.100 M phosphate buffer solution pH = 7.40 between -0.200 V and 0.800 V (10 cycles). It was then modified with the prepared dispersions in the following way: 20  $\mu\text{L}$  aliquot was dropped on top of a polished GCE and the solvent was allowed to evaporate at room temperature.

### Results and Discussion

The pristine GONR material mainly consisted of unzipped multiwall carbon nanotubes, MWCNTs. GONRs is a highly oxygenated material with several types of functional groups, mainly carboxylic, hydroxyl and carbonyl groups. Sample structural characterization has been reported<sup>46,47</sup> previously. Further characterization is given in the following sections.

### Functionalization

Table 1 shows the elemental analysis of raw and functionalized GONRs. GO-PTyr-*in situ* presents the highest nitrogen content and, thus, the highest amount of bound Tyr. This is in accordance with the highest weight loss in TGA (Figure 1), where it is possible to observe an important weight loss centred at 350 °C corresponding to the thermal desorption of PTyr. The bonding of Tyr is higher when the GONR-PTyr was obtained by *in situ* polymerization rather than by covalent linking of commercial PTyr.

GONR-Tyr- $\text{NH}_2$ , GO-Tyr-OH and GO-PTyr-Cov samples show similar TGA profiles, containing a stepwise weight loss that includes the removal of the attached Tyr/PTyr and the oxygenated functional groups that remain after functionalization. As expected, the samples functionalized with Tyr monomers show lower nitrogen content, with the sample GONR-Tyr-OH (amidation reaction) being the one with the lowest nitrogen content. The C/N atomic ratio inversely correlates with the nitrogen content and would indicate that the lowest ratio and highest nitrogen content would correspond to

the highest functionalization degree or in the case of the polymerized sample to the highest tyrosine content.

The TGA profile of the GONRs sample under nitrogen atmosphere (Figure 1) presents three slopes centred at 78°, 185° and 250°C, followed by a gradual weight loss until 800°C. In order to gain an insight into the high oxygen liberation in the functionalized samples and the important weight loss observed at temperatures below 250°C, two control samples were prepared. GONR-Control-T was prepared by refluxing GONRs in DMF at 120°C for 24h with constant magnetic stirring as performed in the esterification reaction. GONR-Control-US was prepared by bath-sonication for 1h in a SDBS aqueous solution (0.5 wt% SDBS in deionized water) as performed in the amidation reaction. Elemental analysis of the control samples is shown in Table 1.

Table 2, shows the weight loss at different temperature intervals for pristine GONRs, control samples and Tyr/PTyr-bonded GONRs. The highest weight loss among GONRs samples corresponds to the pristine GONRs and control samples. The weight loss for GONR-Control-T sample decreases considerably when compared to the pristine GONRs sample and matches with the important loss of oxygen originated by refluxing at 120°C for 24 hours, see Table 2. The total weight loss for the GONR-Control-US sample is slightly lower than for the pristine GONRs sample and also matches the low oxygen loss during the ultrasonication process. The weight loss for GONR-Tyr-NH<sub>2</sub> and GONR-PTyr-Cov samples below 250°C is lower than that for the GONR-Tyr-OH sample indicating that in addition to the mass removal by sonication and refluxing (see control samples), the esterification reactions or/and the Boc cleavage reactions released more oxygenated functional groups than amidation reaction plus CH<sub>3</sub> groups cleavage did. The GONR-PTyr-*in situ* sample, produced from the GONR-Tyr-NH<sub>2</sub> sample, also shows very low weight loss below 250°C.

The GONR-Control-T sample shows a similar TGA profile to that of the pristine GONRs with two slopes centred at lower temperatures than for the GONRs, at 50°C and 158°C, respectively. The weight loss until 250°C is lower in accordance with the oxygen loss during refluxing at 120°C for 24 h. In spite of the low oxygen loss during US treatment, the GONR-Control-US sample shows a modified TGA profile with an only single slope below 200°C.

To gain further insight into the nature of the gases that evolve in the first stage of heating GONR materials, TGA/MS was carried out in independent experiments under Ar atmosphere at 10°C/min on GONR, GONR-Control-T and GONR-Control-US samples. Figure 2 depicts the mass spectra of pristine GONRs and control samples between room temperature and 800°C. Water ( $m/z=18$ ), CO ( $m/z=28$ ), NO ( $m/z=30$ ), H<sub>2</sub>O<sub>2</sub> ( $m/z=34$ ), CO<sub>2</sub> ( $m/z=44$ ), NO<sub>2</sub> ( $m/z=46$ ), SO ( $m/z=48$ ) and SO<sub>2</sub> ( $m/z=64$ ) were registered to elucidate whether the gases released at low temperature came from the reagents used in the preparation of pristine GONRs and/or from solvents such as DMF (GONR-Control T or H<sub>2</sub>O-SDBS (GONR-Control-US). Figure 2 shows the registered signals for H<sub>2</sub>O, CO, CO<sub>2</sub> and NO from the gases

evolved; the rest of the species appeared only at trace levels and were not plotted. It can be seen that for up to 250°C the weight loss can be assigned to water, CO<sub>2</sub> and CO release. At higher temperatures the weight loss is dominated by CO and CO<sub>2</sub> formation. The main weight loss is caused by water for the three samples. Pristine GONRs sample, shows two water peaks centered at 90 and 194°C, GONR-Control-T at 62 and 170°C and GONR-Control-US shows an only wider peak centered at 84°C that evolves between room temperature and 174°C. Eigler et al.<sup>48</sup> reported that it seems likely that breaking GO sheets by sonication generates dangling bonds that are hydrated by the aqueous solvent but not oxidized. The evolution of such breakage with sonication time was studied by measuring the average particle size with dynamic light scattering. It was found that there is a visible decrease in particle size during the first 30min of bath sonication, from about 190 nm to 100 nm, so the scission of GONRs by ultrasounds actually takes place, approximately halving their overall dimensions. Then, from 30min to 120 min, there is no significant change in the average size (Figure S2, Supplementary Information). CO and CO<sub>2</sub> release shows maxima at around 194°C for pristine GONR sample and 184°C for GONR-Control-T. For GONR-Control-US the maxima occurs at a lower temperature and in a smaller amount than for pristine GONR and GONR-Control-T. CO liberation from this sample, increases considerably from 600°C onwards pointing to some rearrangement of the oxygenated functional. At this high temperatures the functional groups that evolve as CO are phenols, quinones, ketones and ether. We hypothesize this to be due to a possible oxidation undergone by GONRs in which the water released along the whole heating program would act as oxidant at high temperatures, inserting a certain amount of oxygen species that are later desorbed from 600°C. These oxidized groups are not present in the initial sample GONR-Control-T but are produced in the heating process. For this reason there is not increase of oxygen content in the sample regarding to pristine GONR sample and are not observed in FTIR and XPS spectra.

Eigler et al.<sup>48</sup> have studied the role of intercalated water in multilayered graphite and have reported the existence of a compound termed as CO<sub>2</sub>-intercalated GO formed between 50 and 120°C by decarboxylation, which is predominantly promoted by the water present in the starting material. This phase decomposed with the release of CO<sub>2</sub>, water and CO at about 160°C. In our samples, the simultaneous liberation of H<sub>2</sub>O, CO and CO<sub>2</sub> took place at 194°C in pristine GONRs. The GONR-Control-US sample seemed to trap H<sub>2</sub>O during ultrasonication process. There was more H<sub>2</sub>O evolved, the CO and CO<sub>2</sub> liberated were in much lower quantities and this also took place simultaneously with water but at lower temperatures. This points to the decomposition of the CO<sub>2</sub>-intercalated GO in the presence of H<sub>2</sub>O as reported by Eigler et al.<sup>48</sup>. However the liberation of CO and CO<sub>2</sub> in GONR-Control-T took place later than water. It is possible that the CO<sub>2</sub>-intercalated GO was removed upon refluxing and that this CO and CO<sub>2</sub> liberated came from the decomposition of some labile oxygenated functional groups after the water release by a different

mechanism than those occurring with the previous samples. NO was liberated from GONR-Control-T sample and originates from DMF absorbed during the control sample preparation.

More information on the modification of GONRs during functionalization processes was obtained by FTIR. Figure 3A depicts the FTIR spectra of pristine GONRs, control samples and commercial L-Tyr and Poly-L-Tyr. Figure 3B, shows the spectra of Tyr/PTyr functionalized samples. The FTIR spectrum for the pristine GONRs corresponds to a highly oxidized carbon material, with strong signals in the region of 1100-1300  $\text{cm}^{-1}$  corresponding to different oxygen functional groups (C-O stretching at  $\approx 1100 \text{ cm}^{-1}$ , O-H deformation absorption at  $\approx 1318 \text{ cm}^{-1}$ ). The peak at 1623  $\text{cm}^{-1}$  can be assigned to O-H of adsorbed water and envelopes the signal at about 1600  $\text{cm}^{-1}$  which reflects the skeletal vibration of C=C aromatic stretching of graphene sheets.<sup>49</sup> A peak at 1725  $\text{cm}^{-1}$  due to carbonyl functions (lactone, carboxylic acids) is also present together with the carboxylate ion as observed from the band at 1585  $\text{cm}^{-1}$ .<sup>49</sup> The broad band at  $\approx 3425 \text{ cm}^{-1}$  is associated with hydrogen-bonded hydroxyl groups and the bands at 2920 and 2850  $\text{cm}^{-1}$  correspond to Csp<sup>3</sup>-H stretching in aliphatic -CH<sub>2</sub>- groups.<sup>52</sup> The band at 3117  $\text{cm}^{-1}$  is associated with C-H stretching in aromatic rings, with the peaks at 780  $\text{cm}^{-1}$  and 670  $\text{cm}^{-1}$  ascribed to out of plane aromatic C-H bending. The GONR-Control-T sample, shows a similar FTIR spectrum profile it retains the characteristics peaks of oxygenated functional groups but with much lower intensity. The GONR-Control-US spectrum shows a noticeable increase in the bands at 3400  $\text{cm}^{-1}$  and 1623  $\text{cm}^{-1}$  confirming water adsorption upon sonication as seen in TGA/MS. GONR samples show a very complex spectrum in which several overlapped signals can be present in the 800-1400  $\text{cm}^{-1}$  region: epoxy and oxirane rings<sup>50,51</sup>, aromatic ethers, primary or secondary in plane O-H bending, phenol or tertiary alcohol, OH bending, and C-O stretching<sup>49</sup>. Thus the relative changes of these signals are difficult to evaluate.

After bonding Tyr by means of the amidation reaction, the spectrum corresponding to GONR-Tyr-OH shows the nearly full depletion of the carboxylic band at 1725  $\text{cm}^{-1}$  and of the carboxylate band at 1585  $\text{cm}^{-1}$ . Likewise it is interesting to note the important decrease in the broad band at 3425  $\text{cm}^{-1}$  assigned to hydrogen-bonded hydroxyl groups. The band at 1623  $\text{cm}^{-1}$  becomes more prominent probably including some contribution from the amide band at 1630  $\text{cm}^{-1}$ . The broad band centred at  $\approx 1240 \text{ cm}^{-1}$  corresponding to C-O stretching of phenol groups and the band at  $\approx 1390 \text{ cm}^{-1}$  associated with O-H bending of phenol groups are also present. Upon esterification of GONRs, the IR spectrum of the GONR-Tyr-NH<sub>2</sub> sample shows the carboxylic peak at 1725  $\text{cm}^{-1}$  shifted to 1743  $\text{cm}^{-1}$  due to the ester bonds and the 1654  $\text{cm}^{-1}$  shoulder corresponding to primary amine (N-H bend 1650-1590  $\text{cm}^{-1}$ ) of Tyr, overlapped with the skeletal vibration of C=C aromatic and the carboxylate band. There are also some variations in the relative intensity of the oxygen functionality at 1100-1300  $\text{cm}^{-1}$  as compared to the pristine GONRs that are not a direct consequence of the esterification reaction but due to the removal of functional

groups during the functionalization process and during the cleavage of protective groups. It should be noted that the band at 3425  $\text{cm}^{-1}$  has almost completely disappeared.

After bonding PTyr covalently, the GONR-PTyr-Cov spectrum shows, as the GONR-Tyr-NH<sub>2</sub> spectrum, the band at 1738  $\text{cm}^{-1}$  corresponding to C=O stretching of the ester moieties and the band at 1624  $\text{cm}^{-1}$  of C=O stretching of amides coming from peptide bonds in PTyr. Another amide feature is observed at 1575  $\text{cm}^{-1}$ , corresponding to secondary amine N-H bending<sup>52</sup>. As well as with GONR-Tyr-NH<sub>2</sub> sample, the band at  $\approx 1200 \text{ cm}^{-1}$  associated with phenol groups becomes more prominent than in GONR-Control-T sample owing to the contribution of phenol groups of PTyr. The spectrum of GONR-PolyTyr-*in situ* shows a prominent band at 1513  $\text{cm}^{-1}$  characteristic of the PTyr that appears in polypeptides with aromatic side chains<sup>53</sup>. In addition to this strong band, two more bands characteristics of PTyr, at around 1630  $\text{cm}^{-1}$  and near 1442  $\text{cm}^{-1}$  are also evident. The characteristics bands of Tyr are better defined in the polymerized sample than in the spectrum of GONR-PTyr-Cov due to higher amount of the amino acid. The band at 1632  $\text{cm}^{-1}$  characteristic of the peptidic amines, is overlapped with the C=O stretching mode of amide bonds (1630  $\text{cm}^{-1}$ ). Other features of amide bands appear at 1583  $\text{cm}^{-1}$  (N-H stretching) and 1177  $\text{cm}^{-1}$  (C-N stretching).

To further elucidate the oxygen functionalities of the pristine and functionalized GONRs and control samples, C 1s, and N1s high resolution XPS was performed. The C1s core-level XPS spectra of the different graphene materials were deconvoluted in five main peaks centred around 284.8 eV (graphitic sp<sup>2</sup> C), 286.1 eV (sp<sup>3</sup> C, epoxy, ether and hydroxyl), 287.2 eV (carbonyl), around 289.9 eV (carboxyl and ester) and the fifth component which corresponds to the characteristic satellite peak from the sp<sup>2</sup>-hybridized carbon atoms due to  $\pi-\pi^*$  shakeup features at  $\approx 291 \text{ eV}$ . Table 3 shows the binding energies and the corresponding areas of the deconvoluted peaks corresponding to C1s core spectra. The peak at 284.8 eV, increases for the control samples as compared to pristine GONRs with this increase being particularly high in the GONR-control-T sample. In this sample, there is also a decrease in the peak area at 286.1 eV and in the carbonyl peak (287.2 eV) which indicates the removal of epoxy, hydroxyl, ether and carbonyl groups. The decrease in these peaks is in agreement with the decrease in the oxygen content from 41.6 to 28.3 wt. % (Table 1) and with the decrease in C-O stretching, O-H stretching and in its FTIR spectrum. The increase in the graphitic sp<sup>2</sup> C points to the partial regeneration of the conjugated sp<sup>2</sup> graphene system with the restoration of C=C bonds at the expense of C-OH and C<sub>o</sub>-OH groups.

In addition to the increase in the peak at 284.8 eV, the C 1s spectrum of the GONR-control-US sample shows an important decrease of the signal at 286.1 eV. Given the small decrease in its oxygen content, its FTIR spectrum and the minimum variation of the carbonyl and carboxylic signal in C1s XPS, the decrease of the signal at 286.1 eV seems to be due to the decrease of sp<sup>3</sup> C.

Upon functionalization with Tyr and PTyr, the peak at 284.8 eV decreases to some extent as compared to the control samples. The peak at 286.1 eV in the control samples shift to 286.3 and 286.6 in GONR-Tyr-OH and GONR-PTyr-Cov respectively and increases considerably probably due to the contribution of phenol groups coming from Tyr/PTyr. A new peak is present at 285.7 eV in the GONR-Tyr-NH<sub>2</sub> sample coming from C-N-H bonds<sup>54,55</sup>

The peak of carboxylic groups in pristine GONRs and control samples at  $289.6 \pm 0.3$  eV shift to 288.5 eV in GONR-PTyr-Cov and to 288.6 eV for GONR-Tyr-NH<sub>2</sub> due to the presence of the Tyr/PTyr peak at 288.8 eV and to the ester groups originated from the esterification of the carboxylic groups of the pristine GONR samples with the phenolic OH groups of Tyr/PTyr. The GONR-Tyr OH peak at 288.3 eV is due to the amide bond ( $-\text{HN}-\text{C}=\text{O}$ ).<sup>56</sup> The peaks at *ca.* 291.0 eV are ascribed to the  $\pi-\pi^*$  shake up typical of sp<sup>2</sup> hybridized carbon.<sup>54</sup> These features are not observed in GONRs nor in their derived control samples, but are present in all Tyr/PTyr functionalized samples, pointing again at the effect of phenol presence coming from the attached molecules. At this point, the information coming from elemental analysis, TGA, FTIR and C1s XPS points to the successful covalent attachment of Tyrosine species to GONRs. Further insights into the nature of such covalent linkages have been obtained by N1s core level

Figure 4 shows the deconvoluted N1s XPS spectra of commercial Tyr and PTyr, and GONR Tyr/PTyr functionalized samples. The two peaks at different binding energies indicate that there are two main chemical states of N. The first, at a binding energy of  $\approx 399.8$  eV is attributed to the bond of O=C-NH-C which comes from amide groups, while the second, at 400.7 eV, represents the bond of C-C-NH<sub>2</sub>.<sup>56,57</sup>

In our samples, there was a peak at  $401.5 \pm 0.2$  eV which appeared in the N1s spectrum of Tyr, and which was also present in the N 1s spectra of GONR-Tyr-NH<sub>2</sub>, GONR-Tyr-OH and GONR-PTyr-Cov and was attributed to C-N-H bonds characteristic of primary amines. In addition to the presence of terminal primary amines in GONR-Tyr-NH<sub>2</sub>, this functionality was also present in GONR-Tyr-OH and GONR-PTyr\_Cov. This could be due to different reasons that are discussed in the following.

The peak at  $400 \pm 0.2$  eV appearing in GONR-PTyr-Cov can be attributed to peptidic amides, (O=C-NH-C) components of PTyr backbone. However, there is an unexpected second component located in the C-N-H region that could be explained on the basis of the PTyr chain composition. The commercial PTyr employed for functionalization, as all polypeptides, possess an amine terminus which is proportionally negligible as the sample would contain larger amounts of amides. During the functionalization process, PTyr could have undergone partial hydrolysis by interaction with the halogenated GONRs, thus reducing chain length and increasing the effective number of amine termini.

As for GONR-Tyr-OH and GONR-Tyr-NH<sub>2</sub> samples, exhibit different ratio of both N1s components than initially expected.

GONR-Tyr-NH<sub>2</sub> sample exhibits lower peak area in the C-N-H region (36.1%) than in the amide region (63.9%). This fact may arise from the fact that the Boc cleavage has not been complete, thus the carbamate bonds could be providing this component. Even if the amount of free amines seem much lower, they have shown to suffice for our purpose, without putting into risk the sample with higher HCl concentrations or longer exposure times. GONR-Tyr-OH sample exhibits roughly the opposite trend (59.7% area for C-N-H and 40.3% for amide), which might be ascribable to the predominant reaction mechanism. The C-N-H region could also reflect in this sample the extent of epoxide ring opening, since this path would create secondary amines (Scheme 1, lower branch) contributing to this component. The intended amidation would be represented by the other component and it seems to take place in a sensibly lower extent. These findings not only confirm the covalent bonding of Tyr and PTyr to GONRs, but also shed light into the occurring functionalization outcome.

Raman spectra of raw and functionalized GONR samples and control samples (Figure 5) show three characteristic peaks; the G-band due to E<sub>2g</sub> vibrational mode of sp<sup>2</sup> bonded carbon at 1570 cm<sup>-1</sup>, the intense D-band (1345 cm<sup>-1</sup>) due to the conversion of sp<sup>2</sup> carbons into sp<sup>3</sup> upon oxidation and to the presence of structural defects in sp<sup>2</sup>-conjugated carbon atoms, and the 2D peak at  $\sim 2670$  cm<sup>-1</sup> which is a second order vibration caused by the scattering of phonons at the zone boundary.<sup>58, 59</sup> The change in intensity of the D-band with respect to the G-band has been related to defects and disorder in graphitic materials.<sup>60</sup> The I<sub>G</sub>/I<sub>D</sub> intensity ratio usually decreases after the covalent functionalization of nanostructured carbon materials.<sup>61</sup> The I<sub>G</sub>/I<sub>D</sub> ratio increased considerably in control samples as a consequence of the partial recovery of the conjugated C sp<sup>2</sup> structure as seen by C1s XPS, Table 3. This increase was particularly high for the GONRs-Control-T sample, where the oxygen content decreased to a high extent, Table 1. After bonding covalently monomeric Tyr and PTyr, the I<sub>G</sub>/I<sub>D</sub> intensity ratio (Figure 5) decreased in comparison with the control samples. Oxygen loss (see Table 1) restored the sp<sup>2</sup> structure in GONRs to some extent as seen in the C 1s XPS spectra of control samples that caused the D-band to decrease. Afterwards, through Tyr/PTyr functionalization, content in sp<sup>2</sup> carbons decreased and they were converted into sp<sup>3</sup> (C1s XPS data). A decrease in the I<sub>G</sub>/I<sub>D</sub> intensity ratio was observed upon functionalization. As for GONR-PTyr-*in situ* sample, despite oxygen removal (see elemental analysis and TGA), the higher amount of attached PTyr led to a drastic decrease the G/D intensity ratio, below that of pristine GONRs and the GONR-Tyr-NH<sub>2</sub> sample used for the ring opening polymerization. This sample, exhibited strong baseline deviation due to its fluorescent properties, together with a noisy spectrum. Results in Figure 5 for GONR-PTyr-*in situ* sample are shown after baseline correction and profile smoothing with NGS LabSpec software. The disappearance of the 2D band in this sample. It is also worth highlighting Given the uncommonness of this fact, we made an attempt to understand the underlying event leading to it. The 2D (also known as G') band, ascribed to the D-band

overtone, is indeed ubiquitous in all  $sp^2$ -based carbon materials. It is a second-order band and the process leading to this feature involves two phonons with opposite momentum. It is known to be one of the very few Raman features exhibiting dependence with the laser excitation energy (dispersive behaviour)<sup>62</sup>. Such characteristics make it useful to identify the kind of carbon material depending on the 2D band shape and components, including the possibility to distinguish between single, few and multi-layered graphene/graphite materials<sup>63</sup>. This band is also very sensitive to doping, as demonstrated for carbon nanotubes, where different contributions accounted for n-type or p-type doping<sup>64</sup>. The disappearance of specific components of the 2D band could obey to the removal of heteroatoms (undoping effects), but apparently never leading to a complete disappearance. In contrast, a higher degree of 2D band depletion has been observed upon structural evolution leading to a loss of ordering<sup>65</sup>. A particular example in literature was reported by Robinson et al.<sup>65</sup>, who found a significant loss of Raman bands of supported graphene (in particular the 2D band) after an intense fluorination, which was explained as a significant structure disruption by fluorine. Therefore, Raman spectra with a barely appreciable 2D band correspond either to disrupted  $sp^2$  carbon networks or to a high level of structural disorder (resembling amorphous carbon)<sup>62</sup>. In our case, after observing a full depletion of the 2D band, we discarded the possibility of “amorphization” of our GONRs upon NCA-Tyr polymerization, but were alerted to a possible effect of further  $sp^2$  disruption during the PTyr formation, consistent with the higher degree of grafting in this sample compared to the rest.

In short, the changes in the binding energies of C1s in XPS that correlates with the changes in the  $I_G/I_D$  of Raman spectra, the binding energy corresponding to amide bond at  $400 \pm 0.2$  eV in N1s XPS spectra and the FTIR spectra showing clearly the band at  $1738\text{ cm}^{-1}$  corresponding to C=O stretching of the ester moieties and several amide and amine features unequivocally demonstrate the covalent bonding of Tyr/PTyr to GONRs.

Figure 6 displays TEM images of the pristine GONRs, GONR-Tyr and GONR-PTyr samples at different magnifications. It can be seen that the pristine GONRs (Figure 6 A) are transparent and displays a gauze-like morphology with slight folds. The high transparency of the sample indicates few layered structure and good dispersion of the graphene oxide ribbons. GO-Tyr/PTyr samples show more compact graphene layers due to the significant removal of oxygen functional groups during the functionalization processing that led to stacking of graphene sheets and at the same time the partial wrapping of graphene sheet by Tyr or PTyr. Images of GONR-Tyr-OH, GONR-Tyr-NH<sub>2</sub> and GONR-PTyr samples show similar appearance with low density agglomerates consisting of GONR sheets wrapped in Tyr/PTyr. Higher magnification images of these samples depict areas where it is possible to see graphene sheets at the edges covered by Tyr to a greater (Figure 6F) or lesser (Figure 6D) degree. Images of the GONR-PTyr-*in situ* sample show higher density agglomerates of PTyr (Figures 6I) gathering GONRs with a more entangled morphology, correlating with higher PTyr content wrapping graphene sheets, even at the

edges. At higher magnification (Figure 4J), thinner sheets are visible at the edges of the agglomerates completely wrapped by PTyr. Characterization data evidence the formation of graphene-Tyr/PTyr functionalized hybrid nanomaterials. GONRs seem to preserve their layer structure but some stacking is produced owing to the removal of some initial oxygenated functional groups and to the wrapping of the layers by the aminoacid/homopolymer. *In situ* polymerization of an NCA aminoacid derivative was shown to cause a significantly higher amount of attached Tyr species as compared to the covalent linking of the corresponding commercial homopolymer, which showed a more agglomerated morphology. Given the well-known fluorescent and electrochemical properties of Tyr and its related compounds, and in order to elucidate their potential for biosensing, the produced hybrid nanomaterials were characterized by fluorescence and electrochemistry

### Fluorescence

Figure 7, shows the fluorescence emission spectra of Tyr, PTyr and GONRs functionalized samples (excitation wavelength=275 nm). Fluorescence intensity is quenched by the presence of GONRs, since GONRs, and mainly reduced GONRs, absorb strongly in the whole UV-Vis region, producing a large background absorption, furthermore, absorption maximum of GONRs is very close to the excitation wavelength (see Figure S3). The overlap between the emission wavelengths of Tyr and the absorbance wavelengths of GONRs make these samples much less fluorescent than free Tyr and PTyr. The largest fluorescence intensity corresponds to GONR-PTyr *in-situ*, which is consistent with the higher degree of bound PTyr as seen by elemental analysis and TGA. The observed emission peak wavelength (302 nm), does not differ significantly from the maximum observed in free Tyr and PTyr. Fluorescence for the rest of the samples is very low, with intensity similar to the Raman scattering of the solvent (Figure 7, bottom). GONR-Tyr-NH<sub>2</sub> shows a new fluorescence peak, which appears at 410 nm (see inset in Figure 7 top).

The origin of this peak needs to be clarified, although the most plausible reasons are stabilization of aromatic radicals due to the nearby presence of graphene<sup>66</sup>, and the formation of reaction by-products, which may present fluorescence at other wavelengths. Other weaker fluorescence peaks appear in the rest of the samples. These may be due not only to the previously exposed causes, but also to conformational effects, specifically interactions between tyrosyl residues.<sup>67</sup> The stronger band at 410 nm is probably due to radical stabilization in GO-Tyr-NH<sub>2</sub>, since it is able to delocalize charge in the graphene structure through the ester group. The weaker bands are more likely assigned to conformational effects. However, more work needs to be done in order to find categorical conclusions in this field. Quantum yield was calculated for GONR-PTyr-*in-situ* using Tyrosine as standard (QY=12%), giving a value of 0.92% which is lower than that of Tyr and

PTyr (QY=2.82%), but still good enough for future applications of this hybrid material as fluorescent material and in sensing.

### Electrochemistry.

Figure 8 shows cyclic voltammograms for  $1.0 \times 10^{-3}$  M L-Tyr solution at polished GCE and GCE modified with GONRs for the first and 10<sup>th</sup> cycle. The results were compared to the GCE modified with GONR-Tyr-OH, GONR-Tyr-NH<sub>2</sub>, GONR-PTyr-Cov and GONR-PTyr-*in situ*. At both electrodes, there was only one anodic process at 0.692 V and at 0.719 V (for GCE and GCE-GONR, respectively) due to the irreversible oxidation of Tyr<sup>68</sup>. The oxidation peak current increased almost twice at GCE/GONRs attributed to the increase in the electroactive area. After successive potential scans the current largely decreased as a consequence of the passivation of the electrode due to the oxidation products of L-Tyr. Cyclic voltammograms obtained at GONR-Tyr-NH<sub>2</sub>, GONR-Tyr-OH and GONR-PTyr-*in situ* in 0.100 M phosphate buffer pH 7.40 did not show anodic current peaks (Figures S4-S6 supplementary information). In the case of GONR-Tyr-NH<sub>2</sub>, the phenol group was not available for electrooxidation, therefore, the absence of anodic currents associated with Tyr electrooxidation was considered reasonable. In the case of GE modified with GNR-Tyr-OH, it was highly possible that the amount of phenolic groups is not enough to define the oxidation signal considering that it presented a low degree of functionalization (according to elemental analysis and TGA experiments). With regard to GONR-PTyr-*in situ*, the absence of the anodic process could be attributed to some problems in the charge transfer associated with the orientation of the electroactive phenolic groups or the distance from the Tyr polypeptide chain, which were not adequate for effective oxidation. It is important to remark that the capacitive current was higher for the sample GONR-Tyr-NH<sub>2</sub> compared to GNR-Tyr-OH, indicating that the GONR-Tyr-NH<sub>2</sub> dispersion was more effective, probably as a result of differences in exposed functional groups.

GCE modified with the GONR-PTyr-Cov sample exhibited a different electrochemical performance. Figure 9 displays voltammetric recordings obtained at GCE modified with GONR-PTyr-Cov dispersion at  $0.100 \text{ V s}^{-1}$  in 0.100M phosphate buffer solution pH = 7.40 for the cycles 1 (dashed line) and 10 (solid line). The first cycle shows an oxidation current peak at 0.674 V and a cathodic current peak at 0.100V. The anodic process is associated with the irreversible oxidation of Tyr oxidation while the cathodic peak is due to the reduction of the quinone group generated by a side reaction of the primary oxidation product of Tyr which produces polypeptides involving diol formation and ortho-quinone as a final product.<sup>68-70</sup> For the 10<sup>th</sup> cycle, the voltamperometric profile changes showing a new oxidation peak at 0.200V, the disappearance of the anodic peak at 0.674 V, and the associated cathodic peak at 0.100 V. It is worth noting that the couple observed at lower potentials did not appear when the positive limit of the voltammetric scan (inset Fig.9) was lower than 0.500 V, clearly demonstrating that both are associated with the primary oxidation product of Tyr. The oxidation process at

0.200 V was only observed for the GCE/GONR-PTyr-Cov indicating that the oxidation products of Tyr from PTyr are different from those obtained for the Tyr monomer in solution under our experimental conditions.

The absence of faradaic processes for GO-PolyTyr-*in situ* compared to GO-PolyTyr-Cov could be due to a more folded and compact structure hindering phenol moieties in comparison with GONR-PTyr-Cov.

By assuming that highly-folded arrangements in peptide secondary structures may hide Tyr residues and render them electrochemically inactive (actually, one of the fundamental principles in electrochemical studies on Alzheimer's disease), then GONR-PTyr-*in situ* might present a spatial organization that hinders phenol moieties and turn them non-electroactive. This is a feasible assumption when taking FTIR spectra (Figure 3) into account, where GONR-PTyr-Cov presents amide I and II bands at 1624 and 1575  $\text{cm}^{-1}$  respectively, and GONR-PTyr-*in situ* presents those bands at 1630 and 1513  $\text{cm}^{-1}$ . Amide I bands in polypeptides in a position around 1630  $\text{cm}^{-1}$  are indicative of  $\beta$ -sheet structure,<sup>71</sup> which in fact seems to be the dominant structure in synthetic PTyr.<sup>71</sup> More interestingly, PTyr was found to present a strong dependence between  $\beta$ -sheet conformation and the molecular weight.<sup>71</sup> At higher molecular weights, PTyr shifts from a regular two-dimensional  $\beta$ -sheet arrangement, to a multi-layered three-dimensional highly compact  $\beta$ -sheet structure. A high molecular weight achieved for the *in situ* polymerized system as determined by TEM and TGA, could be a reasonable explanation for the lack of Tyr electroactivity within GONR-PTyr-*in situ*.

Figure 10 (left) shows the effect of the scan rate on the voltammetric behaviour of GCE modified with GONR-PTyr-Cov in a phosphate buffer solution. The relationship between the oxidation peak current and the scan rates is linear between 0.005 and  $0.200 \text{ V s}^{-1}$  as shown in Fig.10 (right) indicating that the reaction on the electrode was a surface-controlled process.

The obtained results are in agreement with those reported by Krysiński et al.<sup>71</sup> on the electrooxidation of poly-L-tyrosine and insulin amyloid fibrils. This behaviour would indicate that the GONR-PTyr-Cov sample could be used as model for the electro-oxidation of  $\beta$ -amyloid as reported by these authors for insulin amyloid, since hydrophobic residues such as tyrosines play an important role in the formation of protein amyloid fibrils.

### Conclusions and Prospect

Tyr and PTyr were covalently attached to GONRs by means of different strategies. Samples functionalized with Tyr monomer showed lower nitrogen content with the GONR-Tyr-OH sample (amidation reaction) having the lowest nitrogen content. The anchoring of Poly-Tyr was higher as the result of performing the ring opening polymerization (GONR-PTyr-*in situ*) than by covalent attachment of PTyr (GONR-PTyr-Cov). GCE modified with covalently functionalized GONR-PTyr sample, allowed the study of the Tyr oxidation. Sample GONR-PTyr-*in*

*situ* showed the largest fluorescence intensity with quantic yield of 0.92 % due to the higher degree of functionalization.

The obtained hybrid nanomaterials could be used as biomaterials for different applications. GONR-Tyr-OH and GO-Tyr-NH<sub>2</sub> could be used as building blocks for nano-engineered platforms, functional surfaces or molecular scaffolds for tissue engineering. These nanomaterials are able to bond other biomolecules or functional components, such as DNA, aptamers or designed peptide receptors through their free OH or NH<sub>2</sub> binding sites. Likewise, these nanomaterials could be used to modify the band gap in electronic applications. As an example, n-type doping of SWCNTs with peptides containing electron-donating aromatic moieties such as tryptophan and Tyr have been reported previously.<sup>72</sup> GONR-PTyr-Cov, was the only platform where the irreversible oxidation process of Tyr and the reduction of the quinone group generated by a side reaction of the primary oxidation product of Tyr was observed. Therefore, the electrochemical analysis of both types of polypeptide-GONRs films (GONR-PTyr-Cov and GONR-PTyr-*in situ*) proved that the electrochemical behaviour of the tyrosine residues is determined by conformational changes and the spatial arrangement of the polypeptide chains. We have rationalized this difference in terms of the variation of the

electrochemical accessibility of Tyr residues in each structure. This system could be exploited as a biophysical tool in the study of the electrochemical oxidability of proteins for the investigation of the accessibility of Tyr residues in natural proteins within the framework of their interaction with the surrounding environment. GONR-PTyr-*in situ* could be studied as a label-free intracellular sensor or fluorescent probe for live cells imaging and for detecting molecular and physical events. However, it would be necessary to further reach a precisely-controlled size, shape, degree of polymerization and surface chemistry, in addition to exploring its resistance to bleaching in order to reach optimal performance.

In summary, we have presented a peptide-graphene hybrid family with great potential for biological and medical applications, whose characteristics can be tailored by choosing the way in which the (poly)peptide is anchored to the carbon nanostructure. As an example, the GONR/PTyr system demonstrates that the attachment of commercial PTyr is useful in electrochemistry and that the *in situ* polymerization retains the fluorescent properties of Tyr to provide a GONR-based fluorescent material. The strategy proposed here can be extended to other aminoacids, homopolypeptides or proteins.

## Acknowledgements

Financial support for this work was provided by projects TEC2010-15736 and PRI-PIBAR-2011-1, by the Spanish MINECO, Project DGA-ESF-T66 CNN by the Government of Aragon (DGA), the European Social Fund (ESF), CONICET, SECyT-UNC, ANPCyT (PICT 2010-1549 and PICT MICINN 2011-2748) MINCyT- Cordoba Argentina).

## Notes and references

<sup>a</sup> Instituto de Carboquímica (CSIC), C/ Miguel Luesma Castán 4, E-50018 Zaragoza, Spain. Phone: +34 976-733977, Fax : +34 976-733318, \*e-mail: mtmartinez@icb.csic.es

<sup>b</sup> Instituto de Investigaciones en Físico Química de Córdoba (INFIQC) CONICET-UNC, Departamento de Físico Química, Facultad de Ciencias Químicas, Universidad Nacional de Córdoba, Ciudad Universitaria, 5000 Córdoba, Argentina.

\*e-mail: grivas@fcq.unc.edu.ar

Electronic Supplementary Information (ESI) available: FTIR spectrum for the NCA-Tyr-OCH<sub>3</sub> derivative, absorbance spectra of GONRs and Tyr/PTyr-functionalized samples and voltammetric profiles of GONR-Tyr-OH, GONR-Tyr-NH<sub>2</sub> and GONR-PTyr *in situ* samples.

- 1 K. S. Novoselov, A. K. Geim, S.V. Morozov, D. Jiang, Y. Zhang, S. V. Dubonos, I. V. Grigorieva and A. A. Firsov. *Science* 2004, **306**, 666.
- 2 A. K. Geim, *Angew. Chem. Int. Ed.* 2011, **50**, 6986.
- 3 K. P. Loh, Q. L. Bao, G. Eda, M. Chhowalla. *Nat. Chem.* 2010, **2**, 1015.
- 4 A. A. Balandin, S Ghosh, W Bao, I. Calizo, D. Teweldebrhan, F. Miao, CN. Lau. *Nano Lett.* 2008, **8**, 902.
- 5 Y. Xuan, Y. Q. Wu, T. Shen, M. Qi, M. A. Capano, J. A. Cooper, and P. D. Yea. *Appl. Phys. Lett.* 2008, **92**, 013101.
- 6 N. O. Weiss, H. Zhou, Hailong, L. Liao, J. Shan , H. Yu, X. Duan. *Adv. Mater.* 2012, **24**, 5782.
- 7 H. Kim, A. A. Adala, C. W. Macosko. *Macromolecules* 2010, **43**, 6515.
- 8 J. D. Roy-Mayhew, *Chem. Rev.* 2014, **114**, 6323.
- 9 X. Cao, Z. Yin, H. Zhang. *Energ. Environ. Sci.* 2014, **7**, 1850.
- 10 Q. He, S. Wu, Z. Yin, H. Zang. *Chem. Sci.* 2012, **3**, 1764-1772.
- 11 T. Kuila, S. Bose, K. Partha, A. K. Mishrab, N.H. Kimc, J. H. Lee. *Biosens Bioelectron.* 2011, **26**, 4637.
- 12 C. Huang, C. Li, G. Shi. *Energ. Environ. Sci.* 2012, **5**, 8848.
- 13 D. K. Dustin. J. M. Tour, *Acc. Chem. Res.* 2013, **46**, 2307.
- 14 J. Chang, G. Zhou, Christensen, E. R. Christensen, R. Heideman, J. Chen. *Anal. Bioanal. Chem.* 2014, **406**, 3957.
- 15 X. H. Deng, H. Tang, J.H. Jiang. *Anal. Bioanal. Chem.* 2014, **406**, 6903.
- 16 E. K. Wujcik, C. N. Monty. *Wiley Interdisciplinary Reviews-Nanomedicine and Nanobiotechnology* 2013, **5**, 233.
- 17 J. Zhu, M. Chen, Q. He, S. Lu, W. Suying, G. Zhanhu. *RSC Adv.* 2013, **3**, 22790.
- 18 X. Zhou, F. Liang, *Curr. Med. Chem.* 2014, **21**, 855.
- 19 H. Shen, L. Zhang, M. Liu, Z. Zhang. *Theranostics* 2012, **2**, 283.
- 20 A. V. Bryksin, A. C. Brown, M. M. Baksh, M.G. Finn, T. H. Barker. *Acta Biomater.* 2014, **10**, 1761.
- 21 H.P. D. Hosseinkhani, D. S. Yu. *Chem. Rev.* 2013, **113**, 4837.
- 22 A. Petrov, G. F. Audette. *WIREs Nanomed. Nanobiotechnol.* 2012, **4**, 575.
- 23 X. Huang, S. Zauscher, B. Klitzman, G. A. Truskey, W.M. Reichert, D.J. Kenan, M.W. Grinstaff. *Ann. Biomed. Eng.* 2010, **38**, 1965.
- 24 A. M. Wojtowicz, A. Shekaran, M. E. Oest, K. M. Dupont, K. L. Templeman, D. W. Huttmacher, R. E. Guldberg, A. J. Garcia. *Biomaterials* 2010, **31**, 2574.

- 25 P. Y. Wang, T. H. Wu, W. B. Tsai, WH Kuo, MJ Wang. *Coll. Surf. B* 2013, **110**, 88.
- 26 C. Li, J. Adamcik, A. Zhangb, R. Mezzenga. *Chem. Commun.* 2011, **47**, 262.
- 27 A. Battigelli, J. Russier, E. Venturelli, C. Fabbro, V. Petronilli, P. Bernardi, T. Da Ros, M. Prato, A. Bianco. *Nanoscale* 2013, **5**, 9110.
- 28 C. G. Salzmann, M. A. H. Ward, R. M. J. Jacobs, G. Tobias, and M. L. H. Green. *J. Phys. Chem. C* 2007, **111**, 18520.
- 29 H.Y. Mao, S. Laurent, W. Chen, O. Akhavan, M. Imani, A. A. Ashkarran, M. Mahmoudi. *Chem. Rev.* 2013, **113**, 3407.
- 30 A. Sengupta, S. T. Lopina. *J. Biomater. Sci. Polym.* 2002, **13**, 1093.
- 31 A. Sengupta, S. T. Lopina. *Polymer* 2005, **46**, 2133.
- 32 D. Sarkar, J.C. Yang, N. Klettlinger, S. T. Lopina. *eXPRESS Polym. Lett.* 2007, **1**, 724.
- 33 P. N. Shah, Y. H. Yun, J. Biomater. Applications 2013, **27**, 1017.
- 34 J. Huang, C. L. Hastings, G. P. Duffy, H. M. Kelly, J. Raeburn, D. J. Adams, A. Heise. *Biomacromolecules* 2013, **14**, 200.
- 35 M.C. Costache, A.D. Vaughan, H.Qu, P. Ducheyne, D.I. Devore. *Acta Biomater.* 2013, **9**, 6544.
- 36 L. Sheihet, P. Chandra, P. Batheja, D. Devore, J. Kohn, B. Michniak. *Int. J. Pharmaceutics* 2008, **350**, 312.
- 37 A. J. Ditto, P. N. Shah, S.T. Lopina, Y. H. Yun. *Int. J. Pharmaceutics* 2009, **368**, 199.
- 38 A.L. Higginbotham, D.V. Kosynkin, A. Sinitskii, Z. Sun, J.M. Tour, *ACS Nano* 2010, **4**, 2059.
- 39 D.V. Kosynkin, A.L. Higginbotham, A. Sinitskii, J.R. Lomeda, A. Dimiev, B.K. Price, J.M.Tour, *Nature* 2009, **458**, 872.
- 40 A.M. Benito, W.K. Maser, M.T. Martínez. *Int. J. Nanotechnol.* 2005, **2**, 71.
- 41 M-C. Hsiao, S.-H. Liao, M.-Y. Yen, P.-I. Liu, N.-W. Pu, C.-C. M. Ma, *ACS Appl. Mater. Interfaces* 2010, **2**, 3092
- 42 M. E. Jung, M. A. Lyster, *J. Org. Chem.* 1977, **42**, 3761.
- 43 J. Li, W. D. He, L. P. Yang, X. L. Sun, Q. Hua. *Polymer* 2007, **48**, 4352.
- 44 G. J. M. Habraken, M. Peeters, C. H. J. T. Dietz, C. E. Koning, A. Heise, *Polym. Chem.* 2010, **1**, 514.
- 45 J. Cheng, T. J. Deming, *Top. Curr. Chem.* 2012, **310**, 1.
- 46 J. Hernández-Ferrer, P. Laporta, F. Gutiérrez, M. D. Rubianes, G. Rivas, M. T. Martínez. *Electrochem. Commun.* 2014, **39**, 26.
- 47 A. Martn, J. Hernandez-Ferrer, L. Vazquez, M.T. Martinez, A. Escarpa. *RSC Adv.*, 2014, **4**, 132.
- 48 S. Eigler, C. Dotzer, A. Hirsch, M. Enzelberger, P. Muller. *Chem. Mater.* 2012, **24**, 1276.
- 49 J. Coates. *Encyclopedia of Analytical Chemistry*; Meyers, R. A., Ed. John Wiley & Sons Ltd.: Chichester, 2000, 10815.
- 50 C. K. Chua, M. Pumera. *Chem. Eur. J.* 2014, **20**, 1871
- 51 A. M. Dimiev, L. B. Alemany, J. M. Tour, *ACS Nano* 2013, **7**, 576-588.
- 52 A. D. Cross, R. A. Jones, *An Introduction to Practical Infrared Spectroscopy*; Butterworths: London, 1969.
- 53 E.G. Bendit. *Biopolymers*, 1967, **5**, 525.
- 54 A. Y. Sheng Eng, H. L. Poh, J. Luxa, Z. Soferb, M. Pumera. *RSC Adv.* 2013, **3**, 10900
- 55 X. Z. Tang, W. Li, Z.Z. Yu, M.A. rafiee, J. Rafiee, F. Yavari, N. Koratkar. *Carbon* 2011, **49**, 1258.
- 56 T. Ramanathan, F. T. Fisher, R. S. Ruoff, and L. C. Brinson. *Chem. Mater.* 2005, **17**, 1290.
- 57 H. Meng, G.X. Sui, P. F. Fang, R. Yang. *Polymer*, 2008, 610.
- 58 L. M. Malard, M. A. Pimenta, G. Dresselhaus, M. S. Dresselhaus. *Phys. Rep.* 2009, **473**, 51.
- 59 M. M. Lucchese, F. Stavale, E. H. M. Ferreira, C. Vilani, M. V. O. Moutinho, R. B. Capaz, C. A. Achete, A. Jorio. *Carbon* 2010, **48**, 1592.
- 60 S. Niyogi, E. Bekyarova, M. E. Itkis, H. Zhang, K. Shepperd, J. Hicks, M. Sprinkle, C. Berger, C. N. Lau, W. A. de Heer, E. H. Conrad, R. C. Haddon. *Nano Lett.* 2010, **10** 4061.
- 61 C. E. Kalmus, D. M. Hercules. *J. Am. Chem. Soc.* 1974, **96**, 449
- 62 M. S. Dresselhaus, A. Jorio, M. Hofmann, G. Dresselhaus, R. Saito, *Nano Lett.* 2010, **10**, 751.
- 63 A. C. Ferrari. *Solid State Commun.* 2007, **143**, 47.
- 64 I. O. Maciel, N. Anderson, M. A. Pimenta, A. Hartschuh, H. Qian, M. Terrones, H. Terrones, J. Campos-Delgado, A. M. Rao, L. Novotny, A. Jorio. *Nature Mater.* 2008, **7**, 878.
- 65 J. T. Robinson, J. S. Burgess, C. E. Junkermeier, S. C. Badescu, T. L. Reinecke, F. K. Perkins, M. K. Zalalutdinov, J. W. Baldwin, J. C. Culbertson, P. E. Sheehan, E. S. Snow, *Nano Lett.* 2010, **10**, 3001.
- 66 S. S. Lehrer, G. D. Fasman. *Biopolymers* 1964, **2**, 199.
- 67 G. A. Rivas, V. M. Solis. *Anal. Chem.*, 1991, **63**, 2762.
- 68 H. E. Auer, R. P. McKnight *Biochemistry* 1978, **17**, 2798.
- 69 P. R. Abu Nader, P. I. Ortiz, H. A. Mottola. *Anal. Chim. Acta*, 1991, **249**, 395.
- 70 N. A. Nevskaya, Y. N. Chirgadze, *Biopolymers* 1976, **15**, 637.
- 71 A. Lokszejn, W. Dzwolak, P. Krysinski. *Bioelectrochemistry* 2008, **72**, 34.
- 72 D. R. Samarajeewa, G. R. Dieckmann, S. O. Nielsen, I. H. Musselman. *Carbon* 2013, **57**, 88.

## ARTICLE

**Table 1.** Elemental analysis of GONRs, GONR-Control-T, GONR-Control-US, GONR-Tyr and GONR-PTyr samples

Sample	C (wt.%)	H (wt.%)	N (wt.%)	S (wt.%)	O (wt.%)	C/N at. ratio
GONRs	55.1	2.2	0.1	1.0	41.6	642.9
GONR-Control-120	68.1	3.0	0.3	0.3	28.3	283
GONR-Control-US	54.6	2.2	0.2	1.6	41.3	446
GONR-Tyr-NH <sub>2</sub>	73.7	1.5	1.3	0.8	22.7	66.1
GONR- Tyr OH	63.4	2.2	0.4	0.6	33.4	184
GONR-PTyr-cov	76.3	1.8	2.4	0.6	18.9	37.1
GONR-PTyr- <i>in situ</i>	69.7	4.6	5.8	0.1	19.8	17.7

**Table 2.-** Weight loss in Nitrogen atmosphere at different temperature range for GONRs, GONR-Control-T, GONR-Control-US, GONR-Tyr and GONR-PTyr samples

Sample	% Weight Loss	% Weight Loss	% Total Weight Loss
	RT-250°C	250°C-800°C	RT-800°C
GONR	41.5	13.9	55.4
GONR-Control 120	24.2	16.0	40.2
GONR-Control US	35.2	17.2	52.4
GONR-Tyr-NH <sub>2</sub>	3.7	27.6	31.3
GONR-Tyr-OH	10.3	19.7	30.0
GONR-PTyr	4.3	20.6	24.9
GONR-Ptyr <i>in situ</i>	0.1	60.1	60.2
L-Tyrosine	0	81.6	81.6
Poly-L-Tyrosine	4.3	61	65.3

**Table 3.-** XPS data of C 1s deconvoluted into 5 peaks. Binding energies and area percentages (in parenthesis)

Sample	C=C graphitic sp <sup>2</sup>	C sp <sup>3</sup> , epoxy, hydroxyl, ether, C-NH <sub>2</sub>	C=O carbonyl	HO-C=O/ RO-C=O Carboxylic-Ester	$\pi$ - $\pi^*$ shake up
<b>GONRs</b>	284.8 (31.8%)	286.1 (20.1%)	287.2 (42.5%)	289.9 (5.6 %)	
<b>GONR-Control-T</b>	284.8 (55.2%)	286.1 (10.2%)	287.1 (28.6%)	289.4 (6%)	
<b>GONR-Control-US</b>	284.8 (44.9%)	286.1 (6.3%)	287.2 (42.8%)	289.9 (6%)	
<b>GONR-Tyr-NH<sub>2</sub></b>	284.8 (38.1%)	285.65 (46.9%)		288.6 (11.2%)	291.2 (3.75%)
<b>GONR-Tyr-OH</b>	284.6 (39.3%)	286.3 (45.7%)		288.3 (4.9%)	290.2 (10.1%)
<b>GONR-PTyr cov</b>	284.8 (40.4%)	286.6 (47.6%)		288.5 (7.2%)	290.7 (4.9 %)
<b>Tyrosine</b>	284.7 (64%)	286.2 (23.4%)		288.8 (7.9%)	291.5 (4.6%)
<b>Poly(L-Tyrosine)</b>	284.5 (64.1 %)	285.6 (24.7%)	287.4 (7.5%)	288.8 (2.3%)	291.3 (1.4%)

Captions of figures

**Scheme 1.** Functionalization of GONRs with L-Tyr monomer following two different pathways..

**Scheme 2.** Functionalization of GONRs with L-Tyr homopolymer by *ex situ* covalent attachment of commercial PTyr (top branch) or by *in situ* polymerized Tyrosine (using an NCA derivative) on GONR-Tyr-NH<sub>2</sub> (bottom branch).

**Figure 1.** Thermogravimetric plots under Nitrogen atmosphere. Top: samples GONRs, GONRs- Control-T, GONRs- Control-US, L-Tyrosine and Poly-L-Tyrosine. Bottom: samples GONR-Tyr-NH<sub>2</sub>, GONR-Tyr-OH, GONR-PTyr Cov and GONR-Ptyr *in situ*

**Figure 2.** TGA/MS spectra of GONRs, GONR-Control-T and GONR-Control-US between room temperature and 800°C in Argon atmosphere

**Figure 3.** FTIR spectra. A) GONRs, GONR-Control-T, GONR-Control\_US, L- Tyrosine and Poly-L-Tyrosine samples. B) GONR-Tyr-NH<sub>2</sub>, GONR-Tyr-OH, GONR-PTyr-Cov and GONR-PTyr-*in situ* sample

**Figure 4.** N 1s XPS spectra of samples a) Tyr, b) PTyr, c) GONR-Tyr-NH<sub>2</sub>, d) GONR-Tyr-OH, d) GONR-PTyr-Cov

**Figure 5.** Raman spectra (532 nm) of ) GONRs, GONR-Control-T, GONR-Control-US, L- Tyrosine, Poly-L-Tyrosine, GONR-Tyr-NH<sub>2</sub>, GONR-Tyr-OH, GONR-PTyr-Cov and GONR-PTyr-*in situ* samples

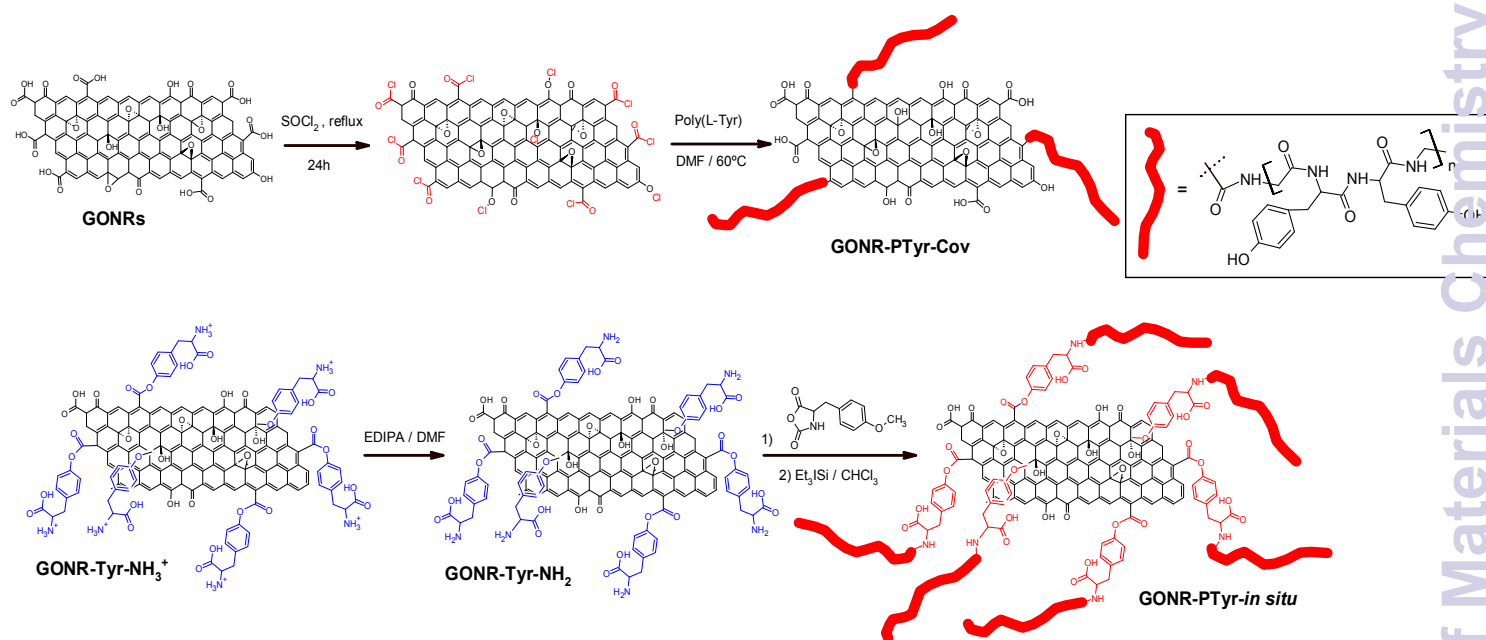
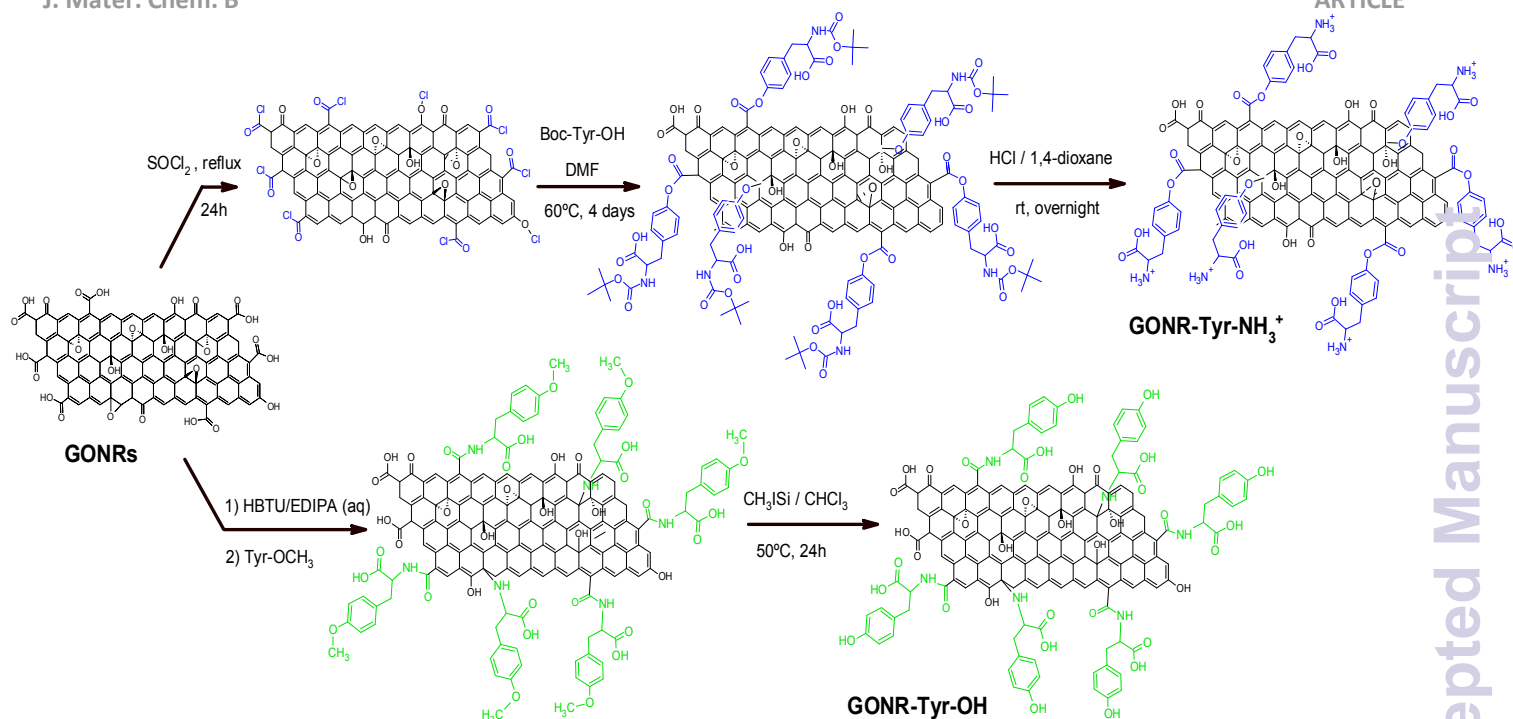
**Figure 6.** TEM images of Figure 6.- TEM images of GONRs (A and B), GONR-Tyr-NH<sub>2</sub> (C and D), GONR-Tyr-OH (E and F),GONR-PolyTyr-cov (G and H) and GONR-PolyTyr-in situ (I and F) at different magnification.

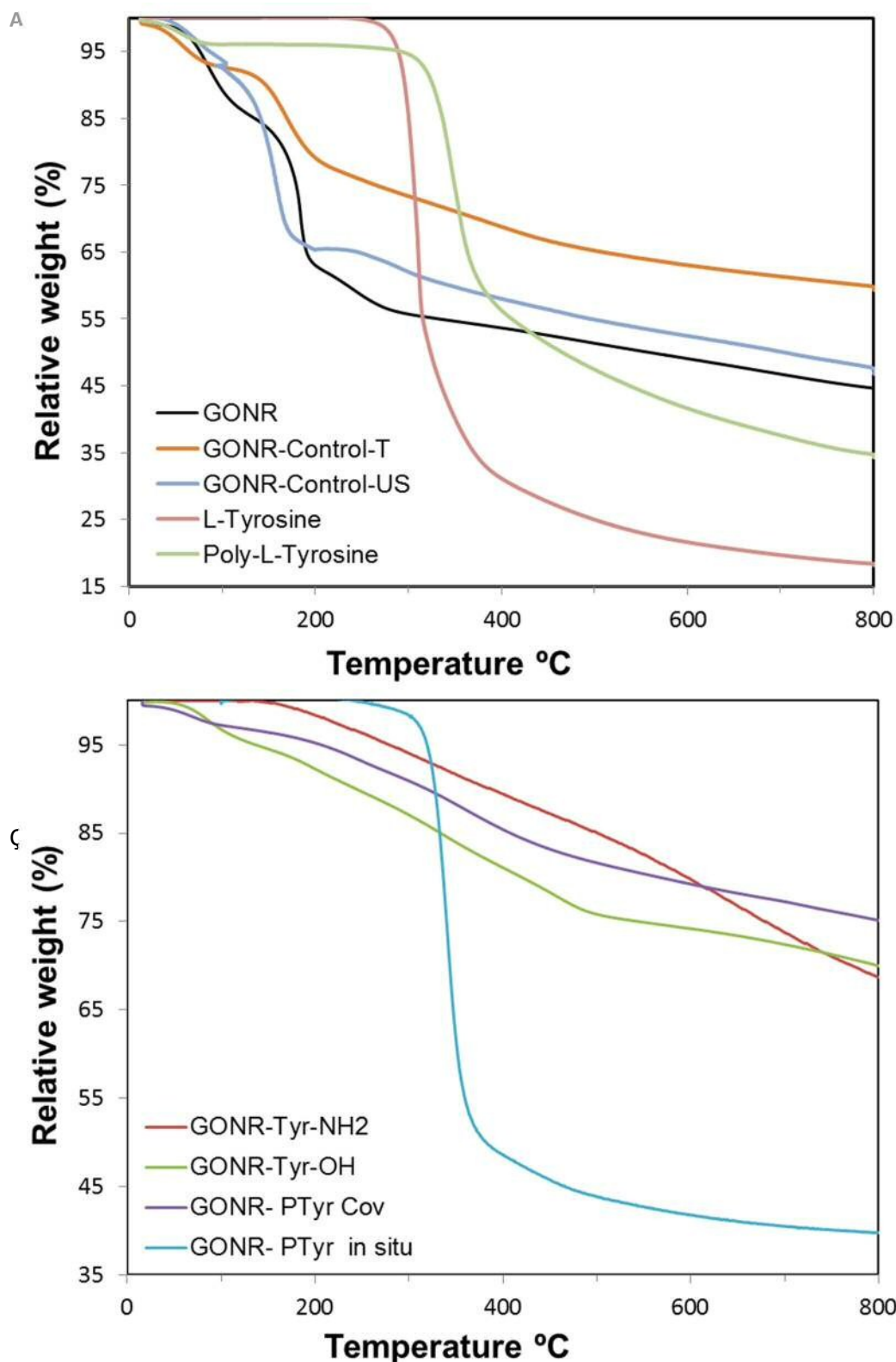
**Figure. 7.** Fluorescence spectra for GONR-Tyr/PTyr samples (Top) and L-Tyrosine/Poly-L-Tyrosine (Bottom)

**Figure 8.** Voltammetric profiles obtained at bare electrode, GCE (left) and GCE modified with GONRs for the first (dashed line) and tenth (solid line) cycle in tyrosine solution 1,0x10<sup>-3</sup>M.

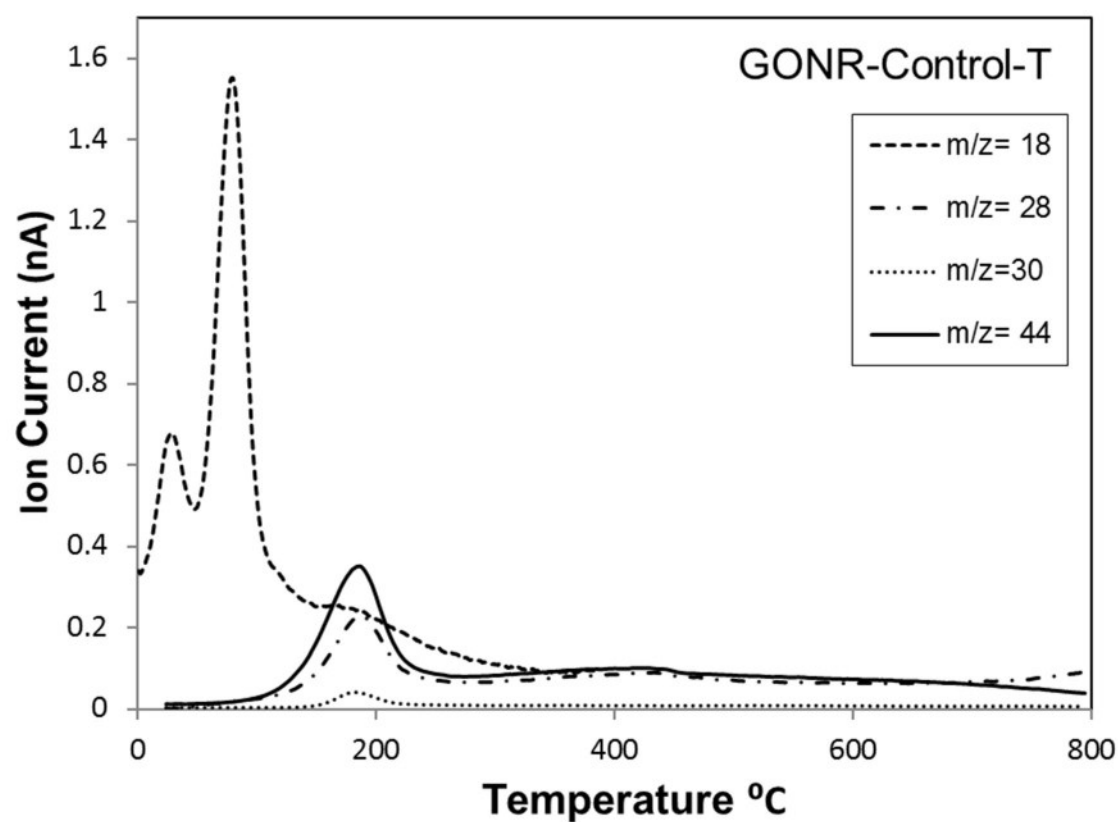
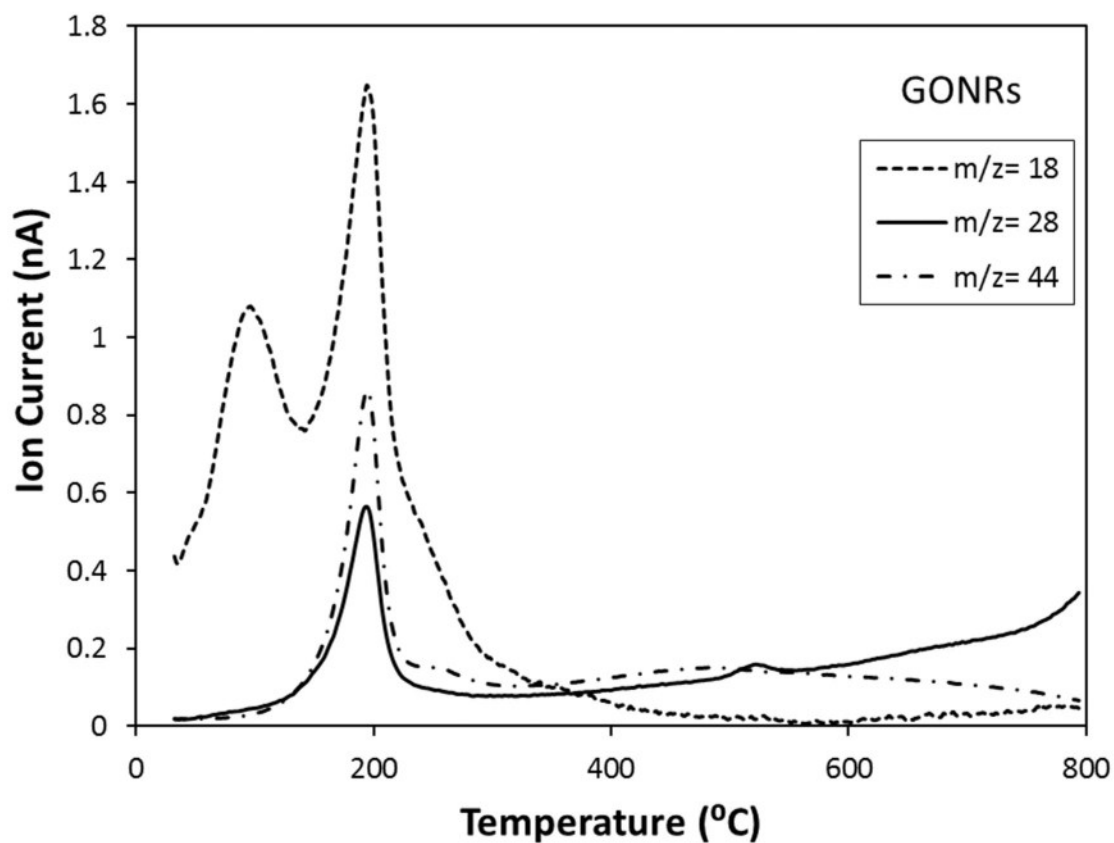
**Figure 9.** Voltammetric response of the GCE/GONR-PTyr for the first (dashed line) and 10<sup>th</sup> (solid line) cycle in buffer phosphate. Inset: Voltammetric profile in a potential window, previous to the tyrosine oxidation

**Figure 10.** Study of the scan rate by cyclic voltamperometry at 0.100 V s<sup>-1</sup> in PBS pH = 7.40 for GCE/GONR-PTyr-Cov. Left: cyclic voltamperograms. Right: oxidation peak current vs. scan rate





**Figure 1.** Thermogravimetric plots under Nitrogen atmosphere. Top: samples GONRs, GONRs- Control-T, GONRs- Control-US, L-Tyrosine and Poly-L-Tyrosine. Bottom: samples GONR-Tyr-NH<sub>2</sub>, GONR-Tyr-OH, GONR-PTyr Cov and GONR-PTyr *in situ*



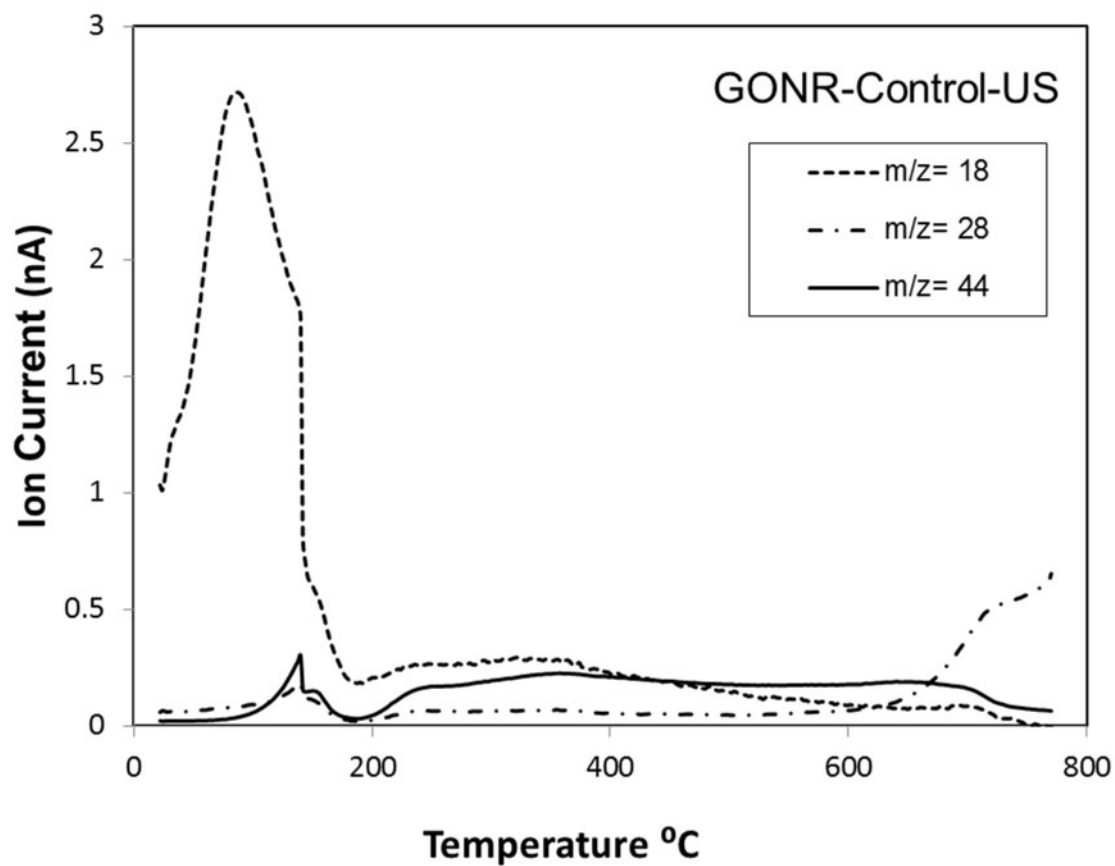
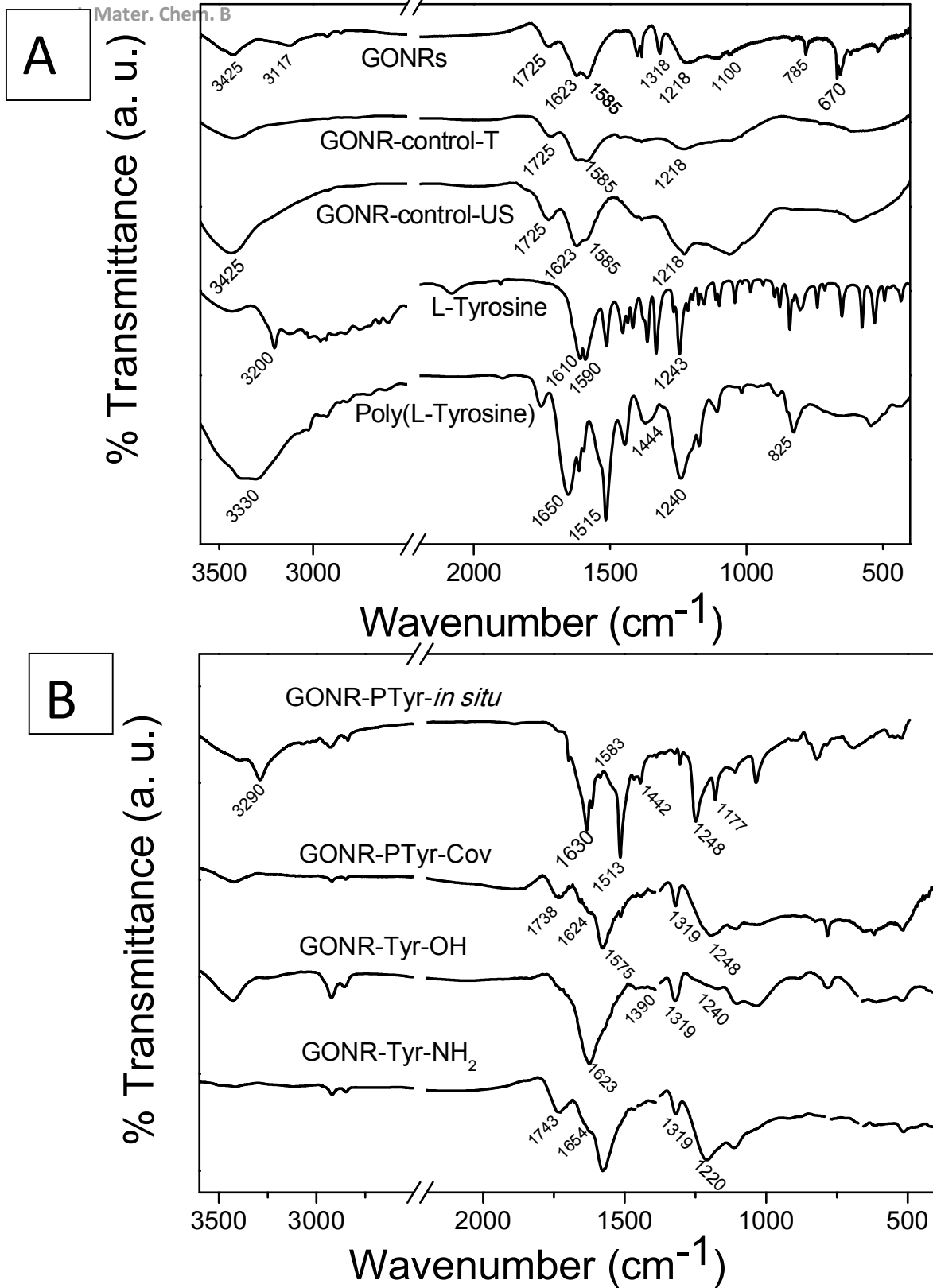


Figure 2.-TGA/MS spectra of GONRs, GONR-Control-T and GONR-Control-US between room temperature and 800°C in Argon atmosphere



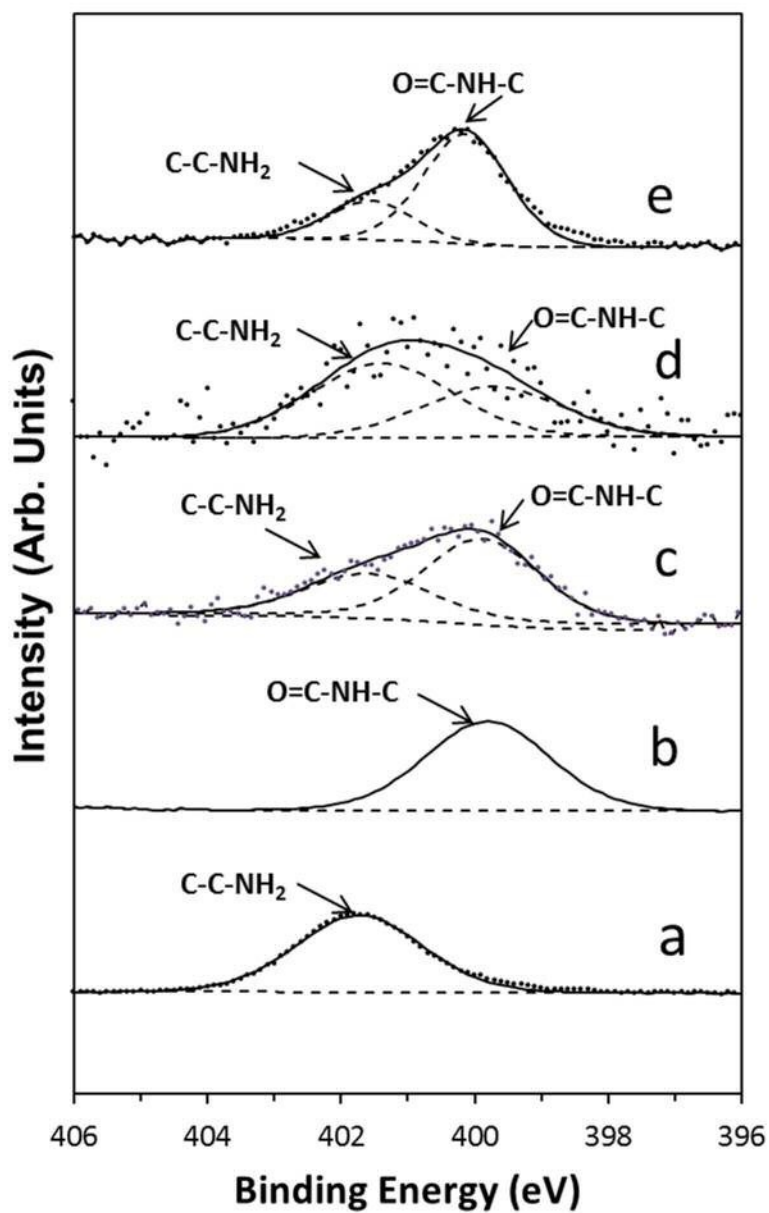


Figure 4. N 1s XPS spectra of samples a) Tyr, b) PTyr, c) GONR-Tyr-NH<sub>2</sub>, d) GONR-Tyr-OH, e) GONR-PTyr-Cov

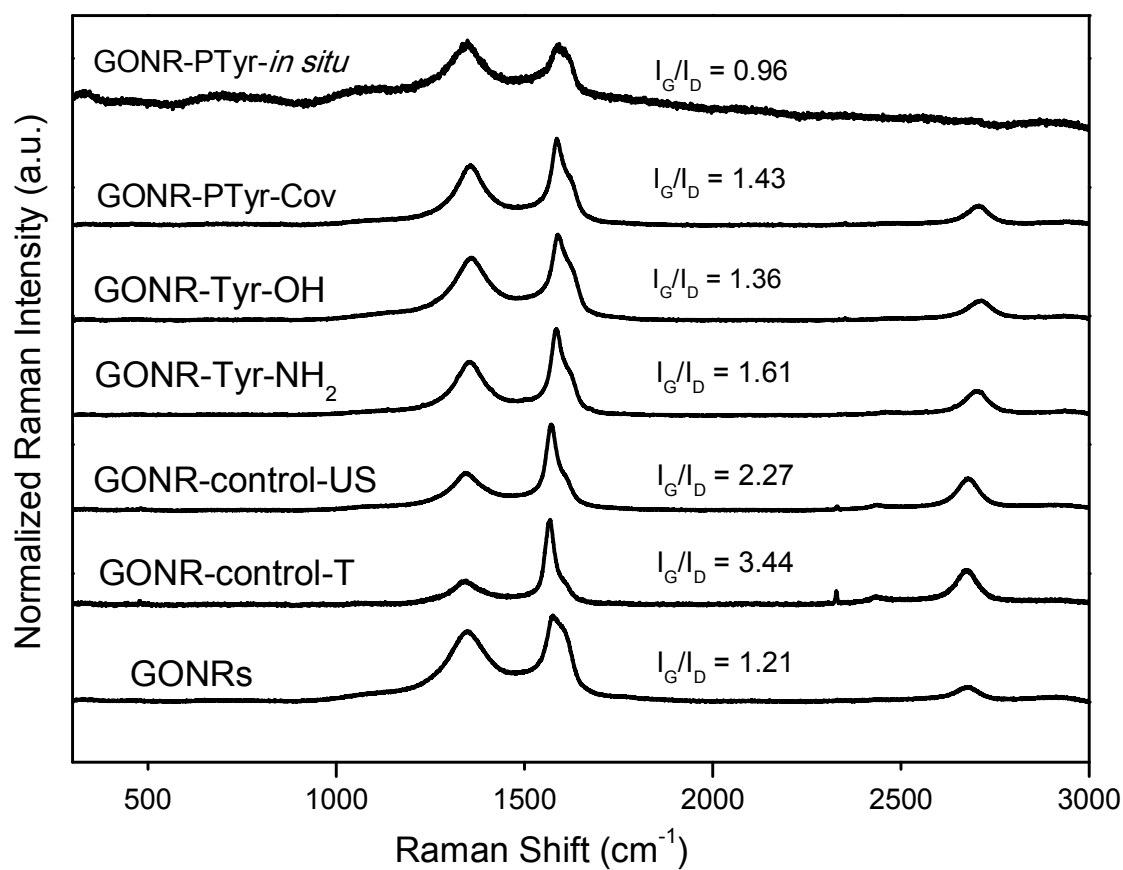
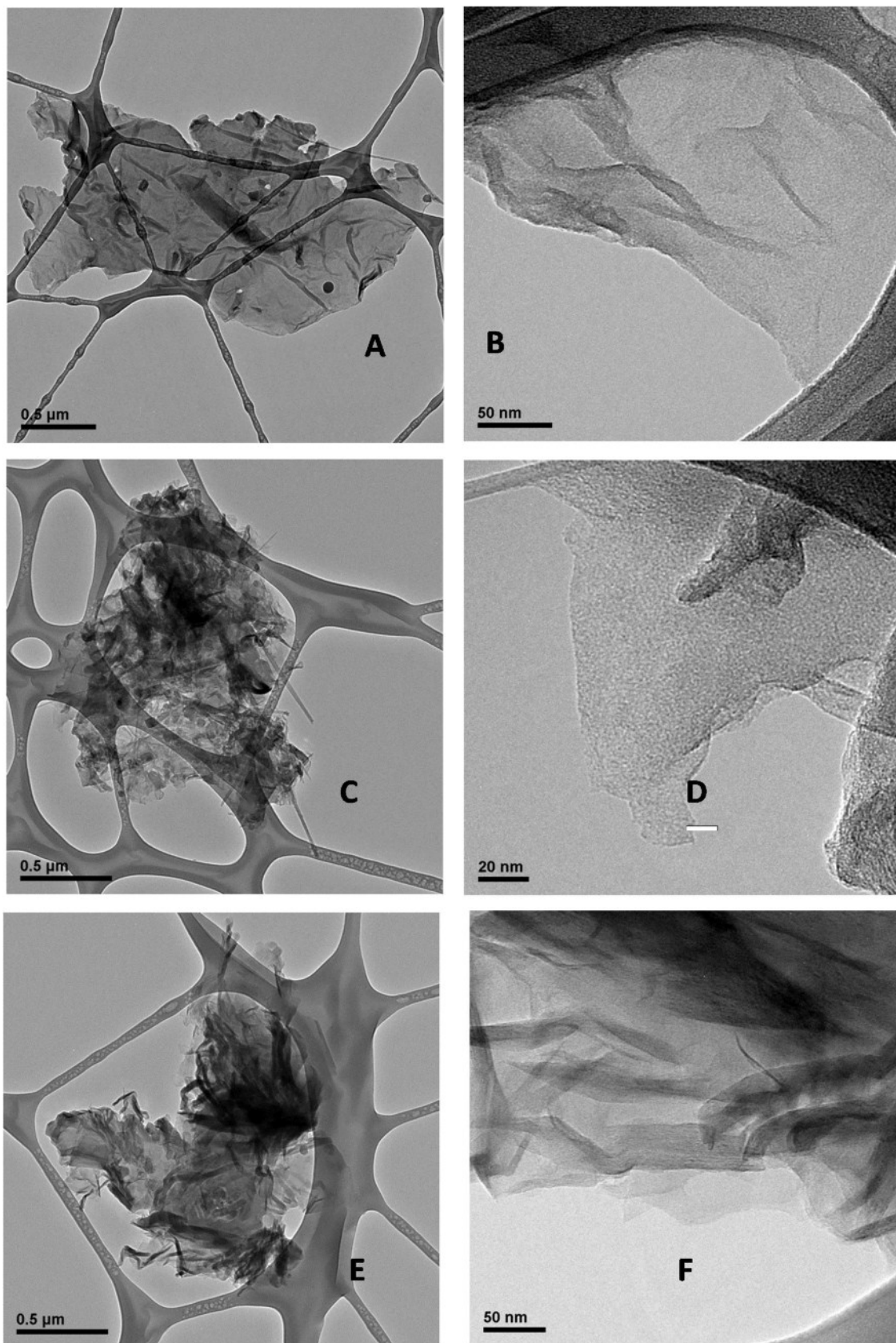


Figure 5.-. Raman spectra (532 nm) of GONRs, GONR-Control-T, GONR-Control-US, L-Tyrosine, Poly-L-Tyrosine, GONR-Tyr-NH<sub>2</sub>, GONR-Tyr-OH, GONR-PTyr-Cov and GONR-PTyr-*in situ* samples



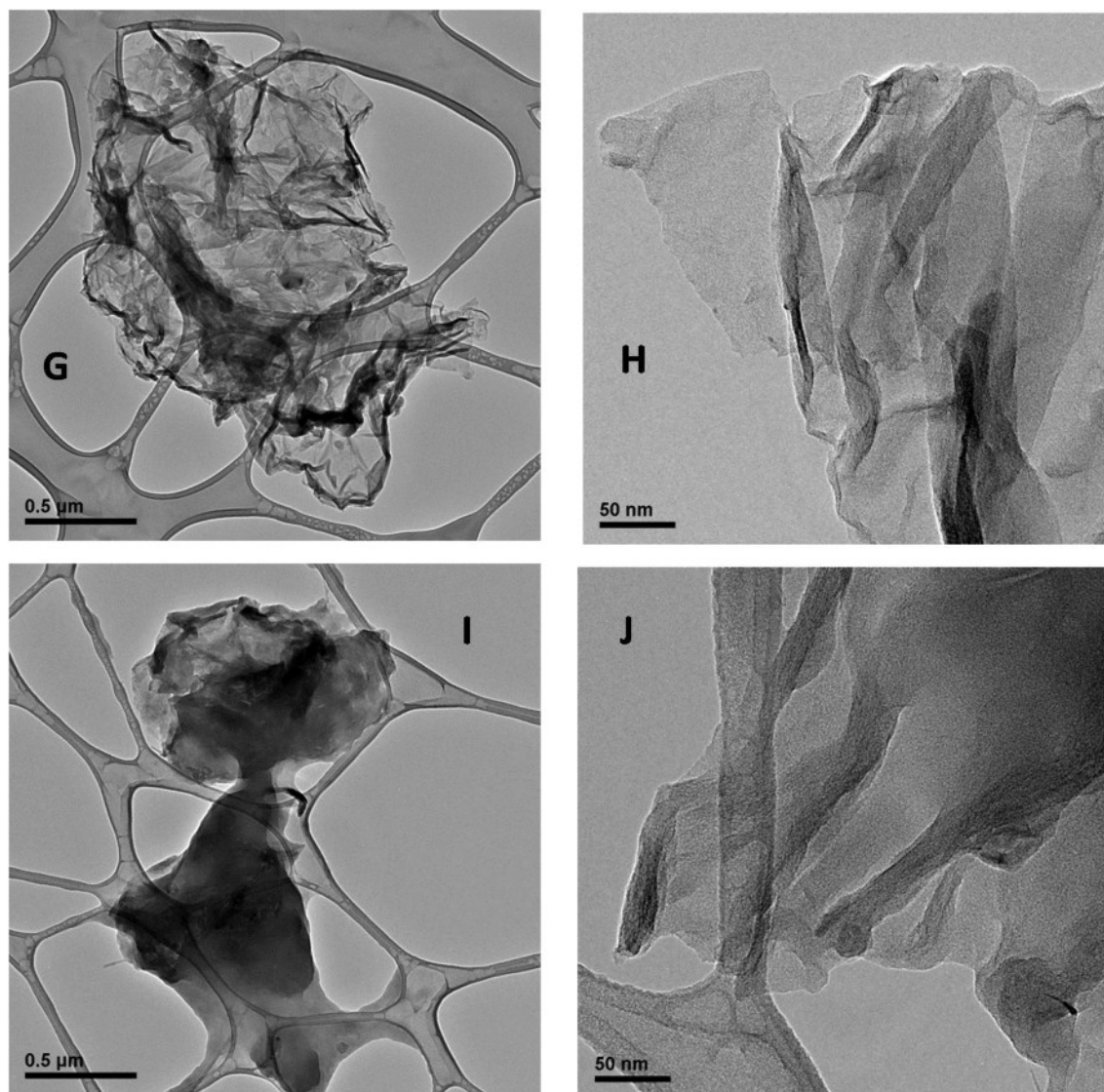


Figure 6.- TEM images of GONRs (A and B), GONR-Tyr-NH<sub>2</sub> (C and D), GONR-Tyr-OH (E and F), GONR-PolyTyr-cov (G and H) and GONR-PolyTyr-in situ (I and F) at different magnification.

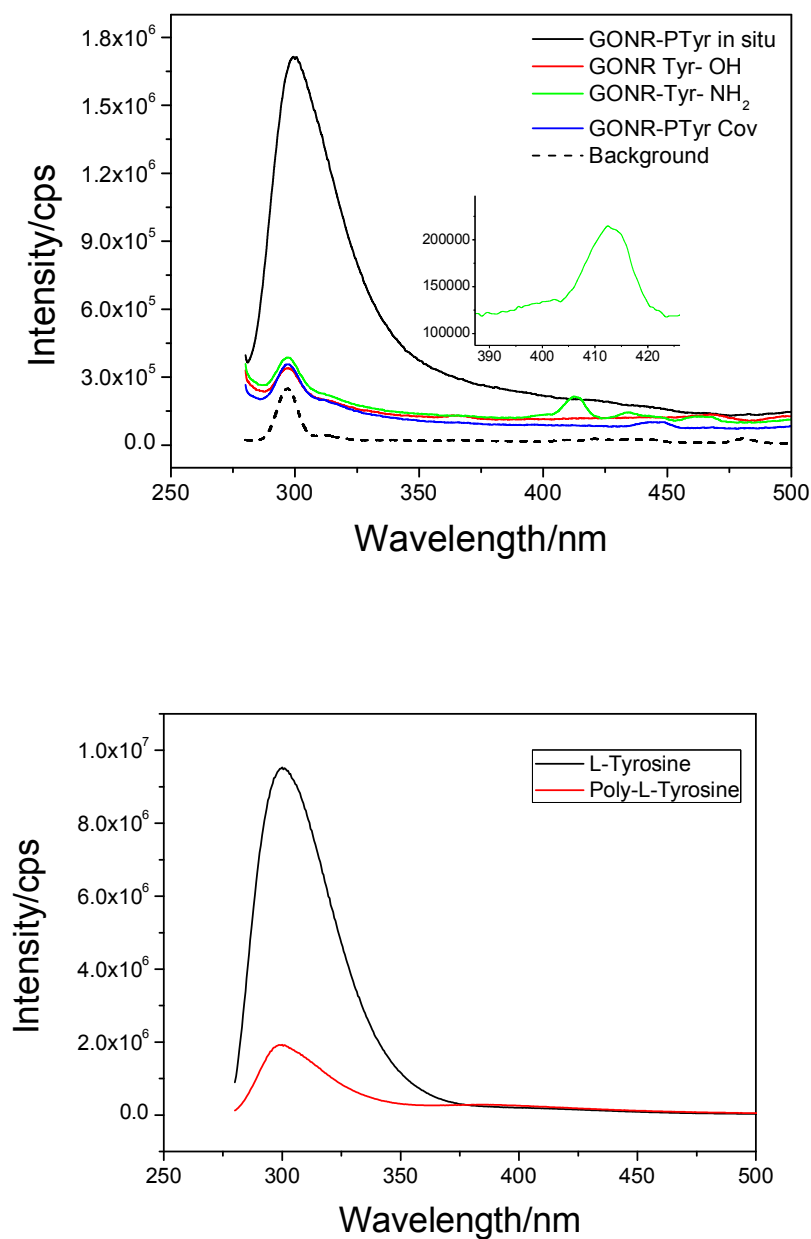
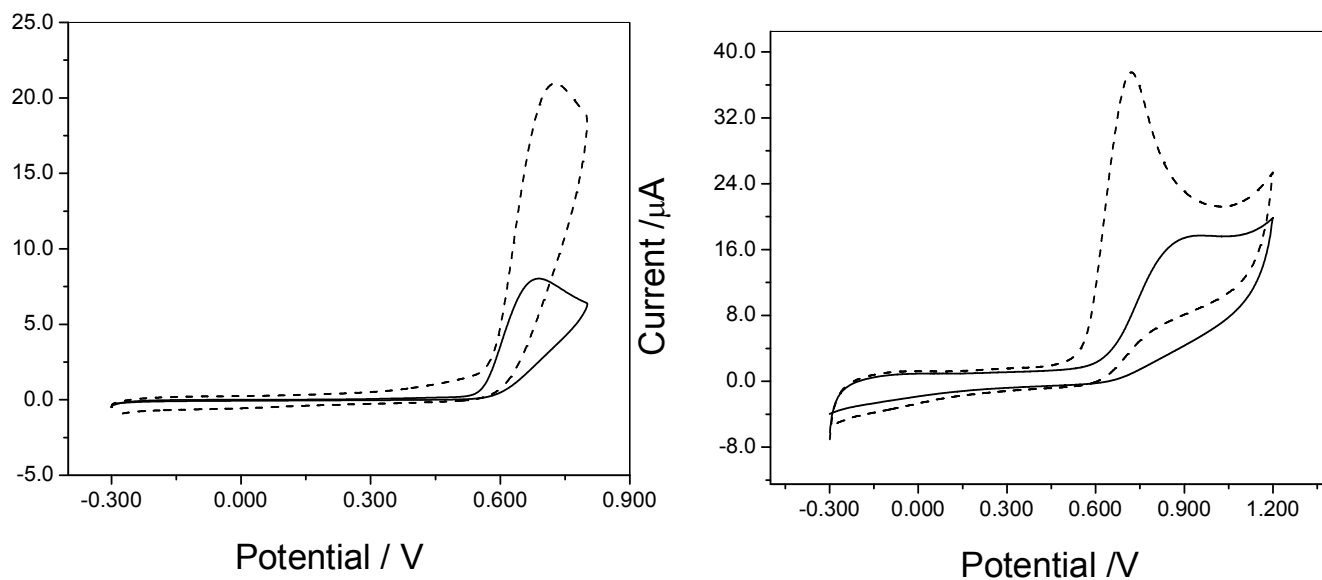
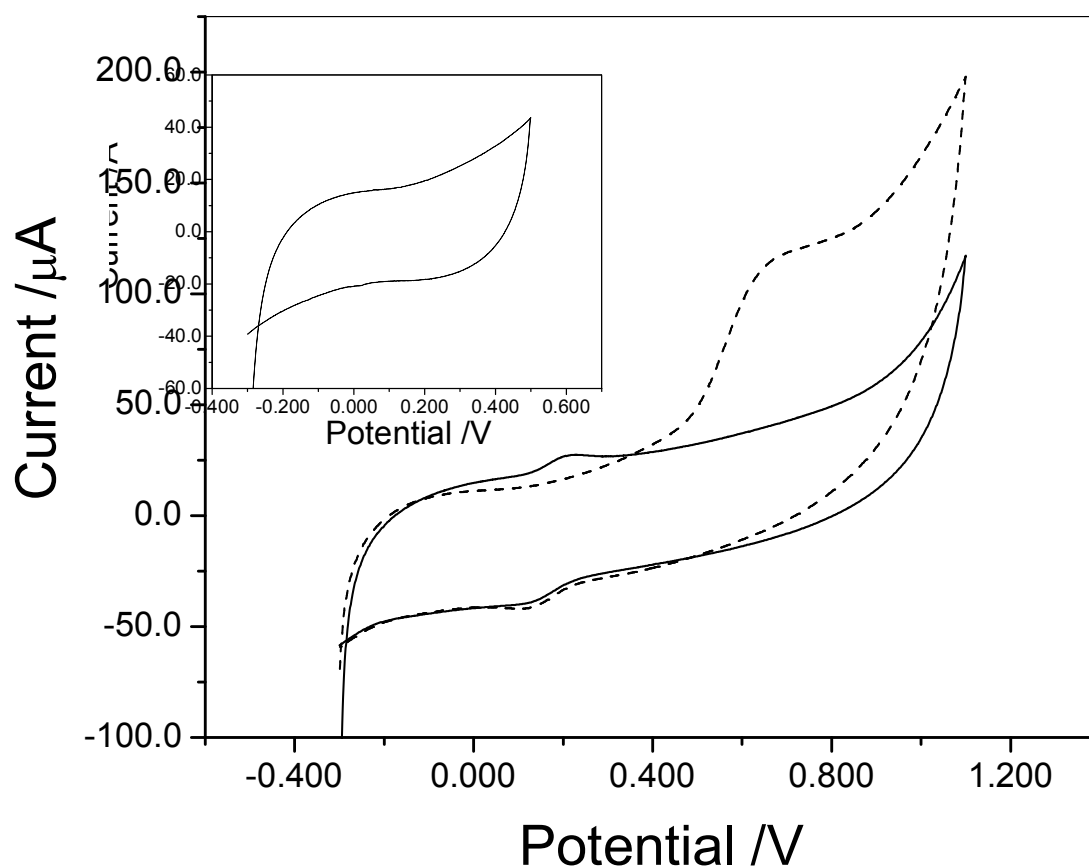


Figure. 7. Fluorescence spectra for GONR-Tyr/PTyr samples (Top) and L-Tyrosine/Poly-L-Tyrosine (Bottom)



**Figure 8.** Voltammetric profiles obtained at bare electrode, GCE (left) and GCE modified with GONRs for the first (dashed line) and tenth (solid line) cycle in tyrosine solution  $1.0 \times 10^{-3}$  M.



**Figure 9.** Voltammetric response of the GCE/GONR-Ptyr-Cov for the first (dashed line) and 10<sup>th</sup> (solid line) cycle in buffer phosphate. Inset: Voltammetric profile in a potential window, previous to the tyrosine oxidation

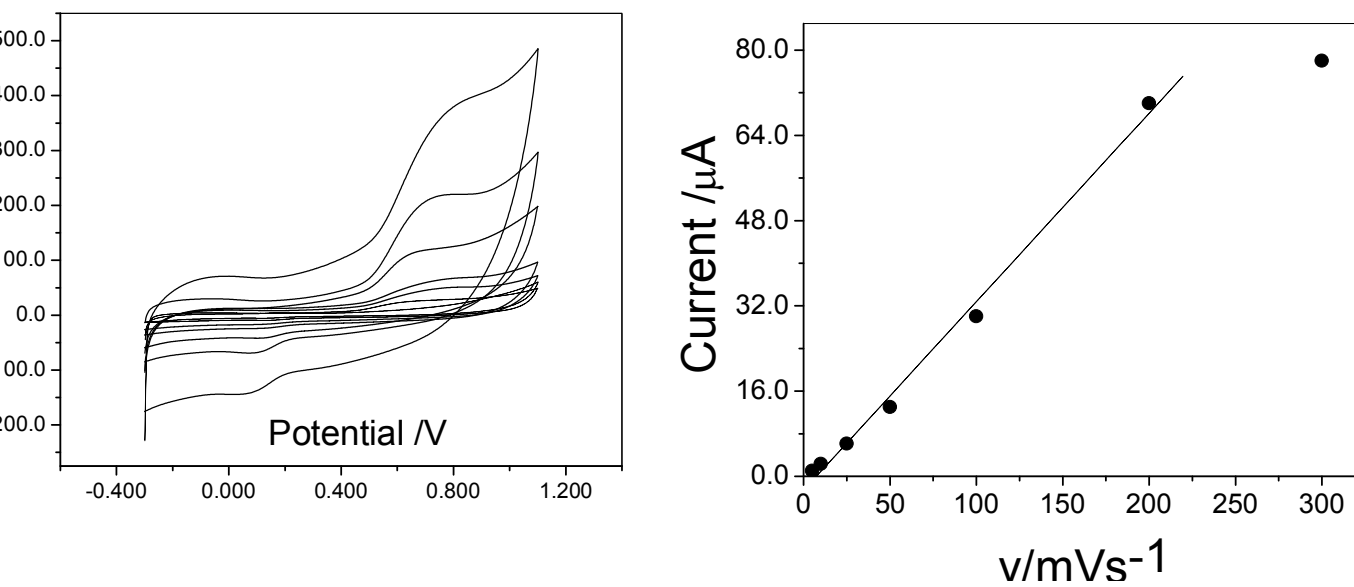


**Figure 10.** Study of the scan rate by cyclic voltamperometry at  $0.100 \text{ V s}^{-1}$  in PBS pH = 7.40 for GCE/GONR-PTyr-Cov. Left: cyclic voltamperograms. Right: oxidation peak current vs. scan rate

## SUPPLEMENTARY INFORMATION

3900 3400 2900 2400 1900 1400 900 400

Wavenumber (cm<sup>-1</sup>)

osine and

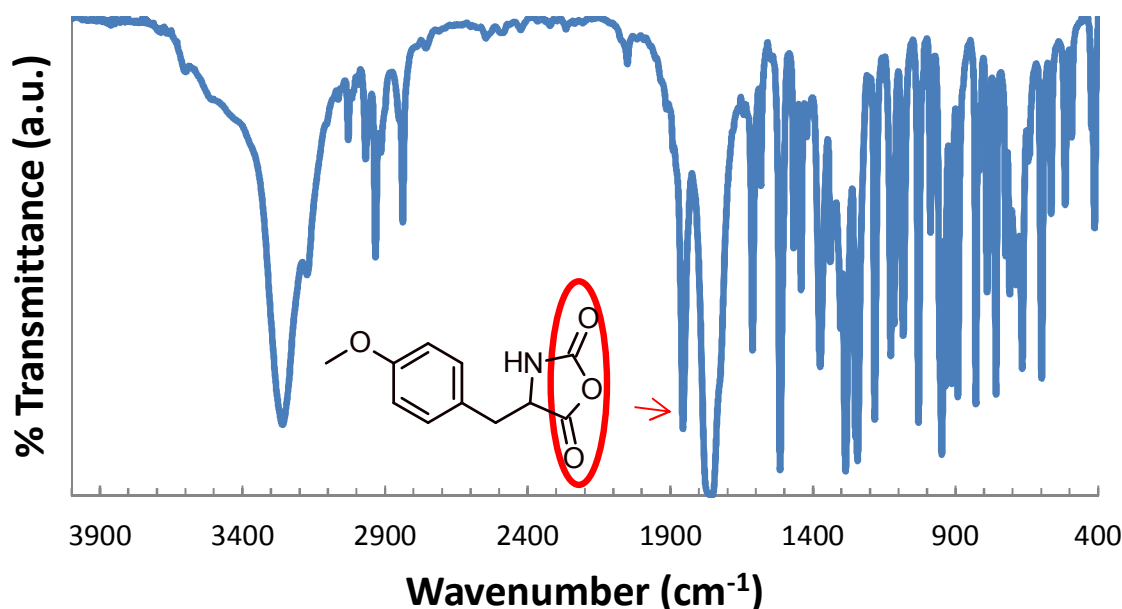
### Poly L-Tyrosine to Graphene Oxide Nanoribbons

J. M. González-Domínguez,<sup>a</sup> F. A. Gutiérrez,<sup>b</sup> J. Hernández,<sup>a</sup> A. Ansón-Casaos,<sup>a</sup> M. D. Rubianes,<sup>b</sup> G. Rivas<sup>b\*</sup> and M. T. Martínez<sup>a\*</sup>

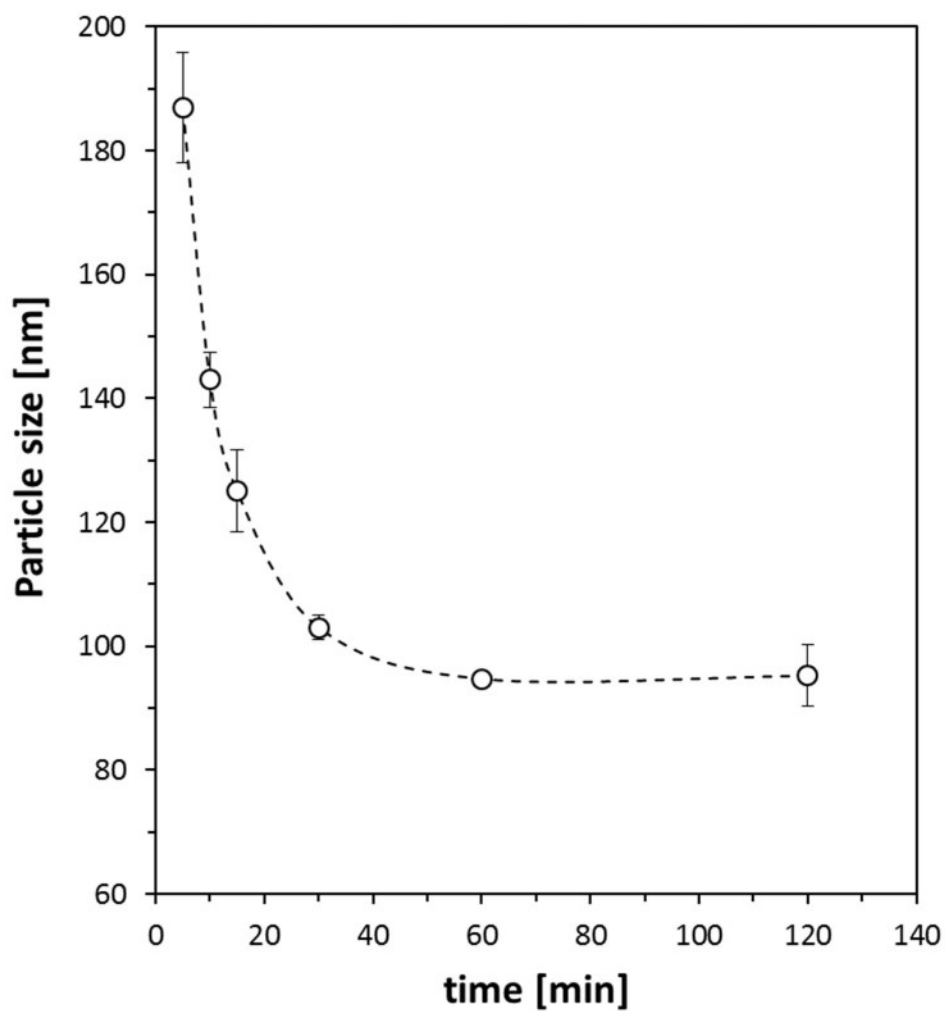
<sup>a</sup> Instituto de Carboquímica (CSIC), C/ Miguel Luesma Castán 4, E-50018 Zaragoza, Spain. Phone: +34 976-733977, Fax: +34 976-733318,

**\*e-mail: [mtmartinez@icb.csic.es](mailto:mtmartinez@icb.csic.es)**

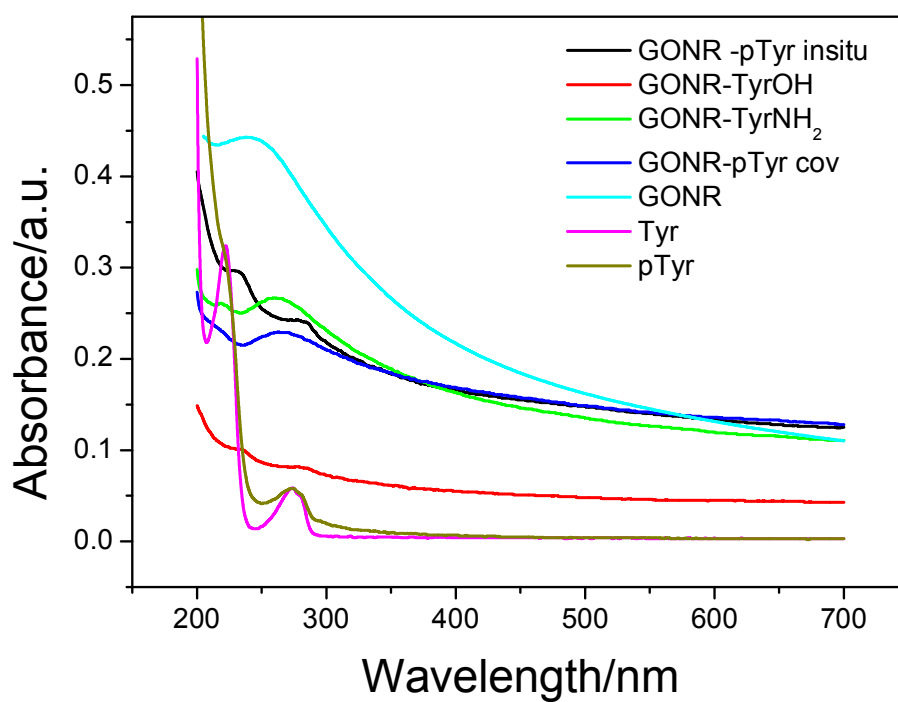
<sup>b</sup> Instituto de Investigaciones en Físico Química de Córdoba (INFIQC) CONICET-UNC, Departamento de Físico Química, Facultad de Ciencias Químicas, Universidad Nacional de Córdoba, Ciudad Universitaria, 5000 Córdoba, Argentina.



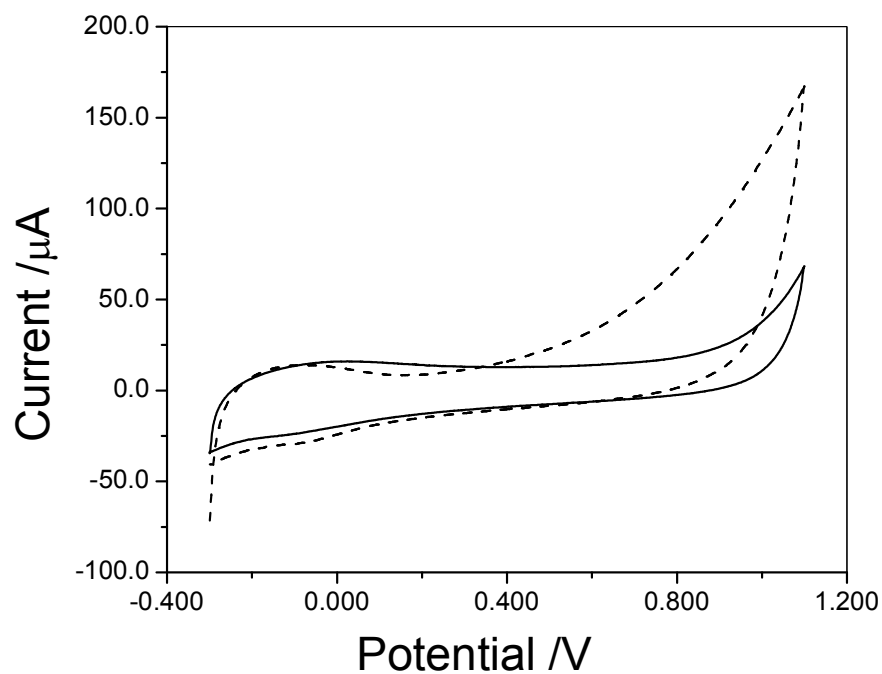
**Figure S1.** FTIR spectrum for the NCA-Tyr-OCH<sub>3</sub> derivative.



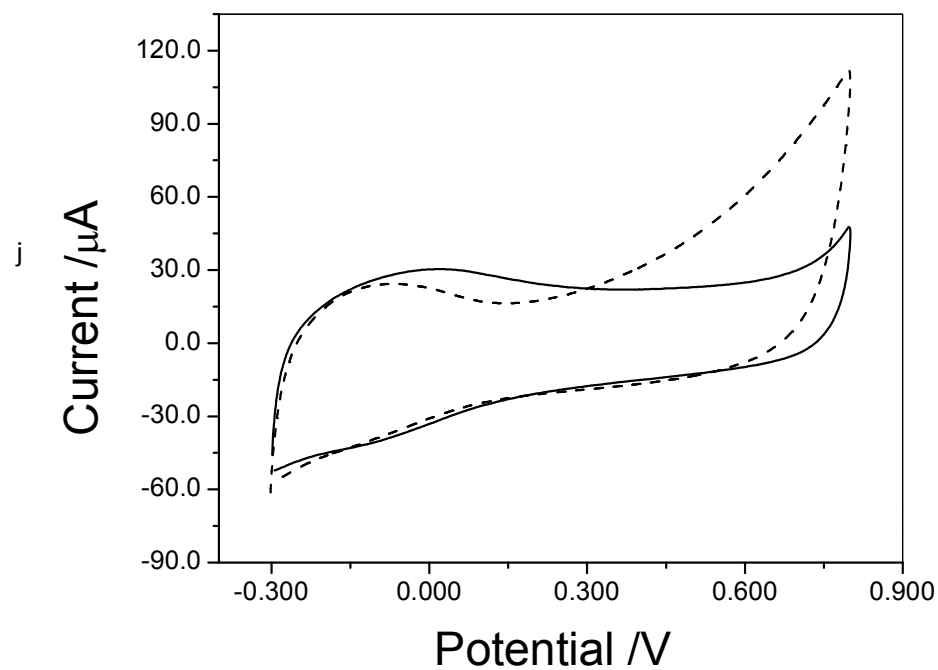
**Figure S2.** - Average particle size versus sonication time



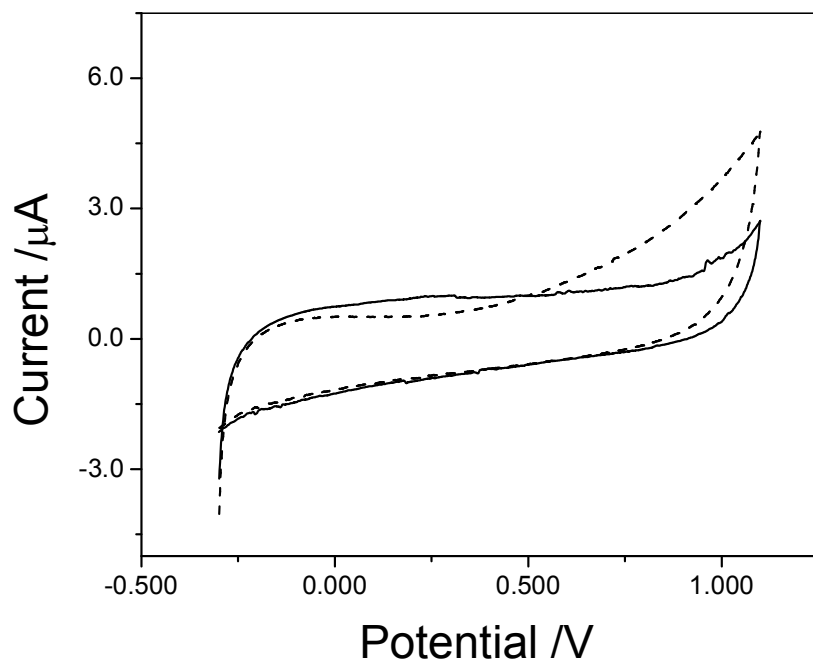
**Figure S3.** Absorbance spectra of pristine GONR and GONR functionalized with Tyr/P



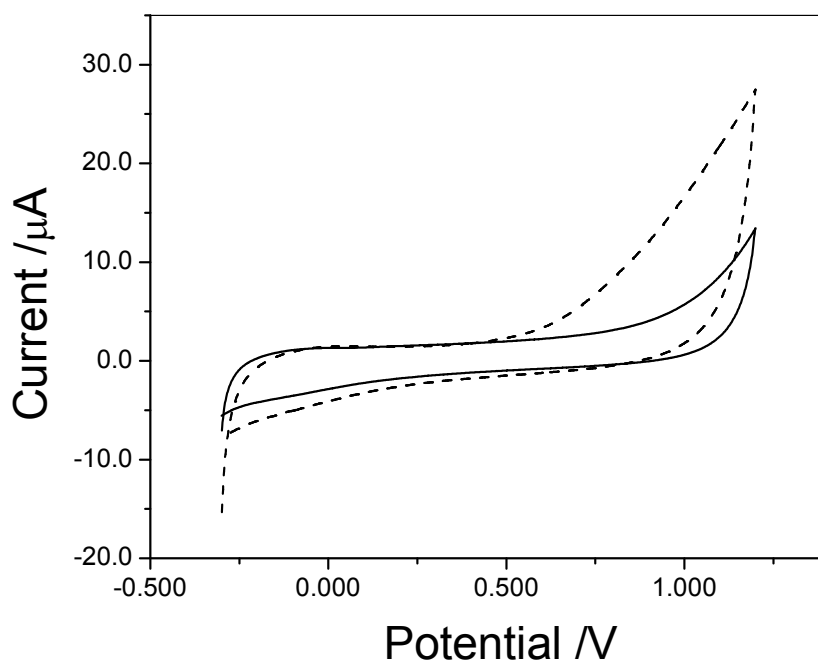
**Figure S4.**- Voltammetric profiles obtained at GCE/ GONR-Tyr-OH for first (-dashed line) and tenth (solid line) in buffer phosphate



**Figure S5.** Voltammetric profiles obtained at GCE/ GONR-Tyr-NH<sub>2</sub> for first (-dashed line) and tenth (solid line) in buffer phosphate.

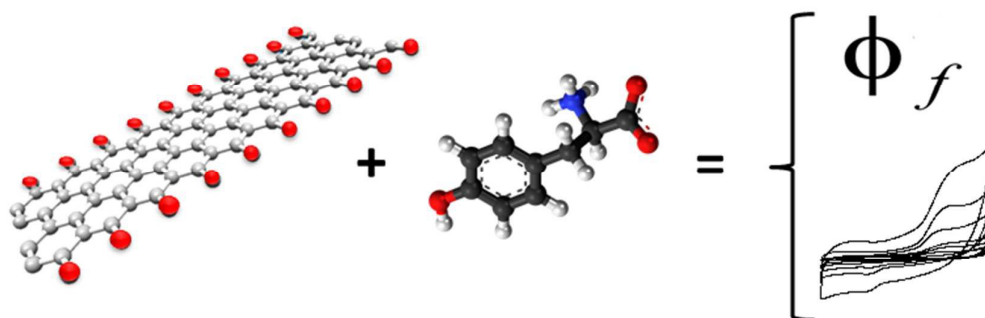


**Figure S6.** Voltammetric profiles obtained at GCE/ GNOR-PTyr “in situ” for first (-dashed line) and tenth (solid line) in buffer phosphate.



**Figure S7.** Voltammetric profiles obtained at GCE/ GONR for first (-dashed line) and tenth (solid line) in buffer phosphate.

## GRAPHICAL ABSTRACT



GONRs grafted to Tyrosine and Poly-Tyrosine can be used as biophysical tool for studying the oxidability of proteins or as fluorescent probe for detecting molecular or physical events